Computer Aided Multiscale Design of SiC-Si_3N_4 Nanoceramic Composites for High-Temperature Structural Applications

PIs: Vikas Tomar and John E Renaud

Aerospace and Mechanical Engineering
University of Notre Dame, Notre Dame-Indiana, USA, 46556

Program Manager: Dr. Patricia Rawls

DoE-NETL UCR Grant DE-FG26-07NT43072

Students

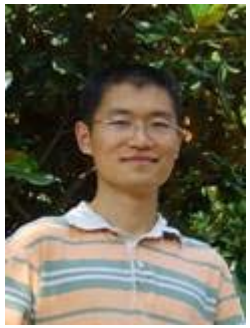

Devendra Dubey, Ming Gan, Vikas Samvedi

Collaborators

John Renaud (Material Design), Raj Bordia (Material Processing and Manufacturing)

Lab Facilities

52 Processor Opteron dual core supercomputing cluster, 8 Terabytes storage server, Veeco AFM, MTS Instron mechanical hydraulic testing machine, Hopkinson bar for dynamic high strain rate testing

Clean Coal Utilization

- The Energy Department's Office of Fossil Energy is working on coal gasifier advances that enhance efficiency, environmental performance, and reliability as well as expand the gasifier's flexibility to process a variety of coals and other feedstocks (including biomass and municipal/industrial wastes).

- Coal gasification is one of the most promising technologies for energy plants of the future.
  - Need materials for high temperature applications.
    - Oxidation, corrosion, creep and fracture resistance.
  - $SiC-Si_3N_4$ composites.

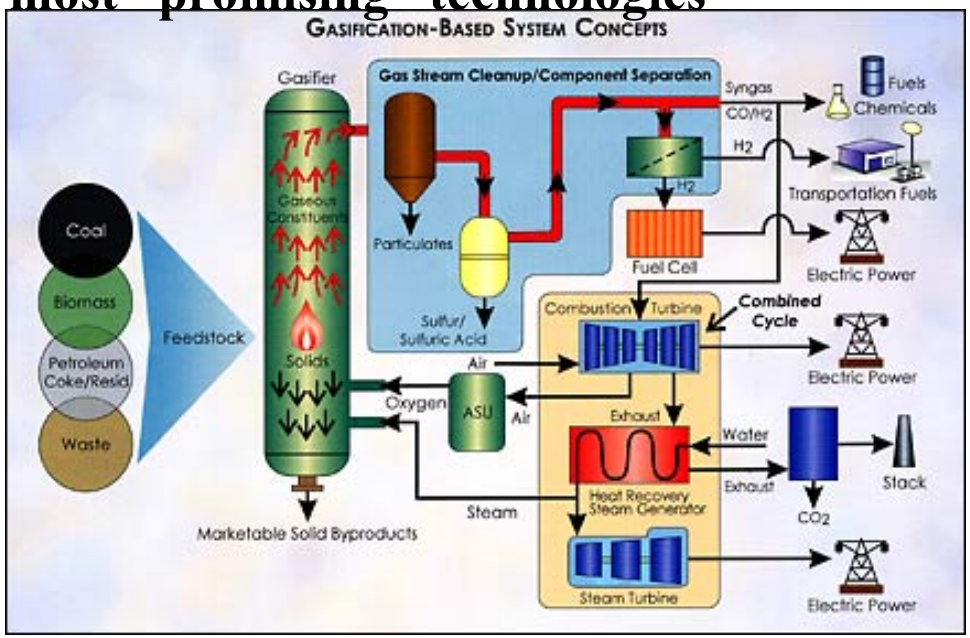

Computer-aided design to investigate materials for use in future high temperature power plant applications

Design Targets

Fracture and creep resistance at about 1200 K

$SiC-Si_3N_4$

Design Variables

- Phase size
- Phase Volume Fraction

Variable Fidelity Optimization

Multiscale Material Simulation

Optimal Morphologies

$SiC-Si_3N_4$ nanocomposite with desired properties

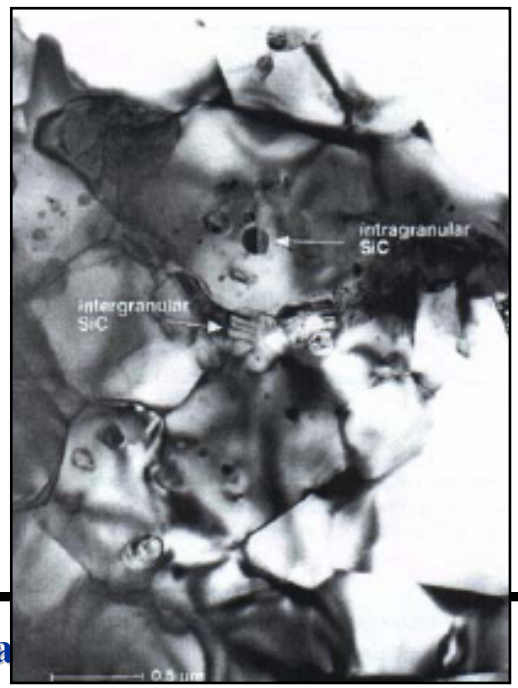

Want: Accuracy of quantum mechanics (QM) in 10^{23} atom systems…

This is impossible (today and in the foreseeable future)

Possible solution:
Multi-scale modeling techniques based on hierarchies of overlapping scales

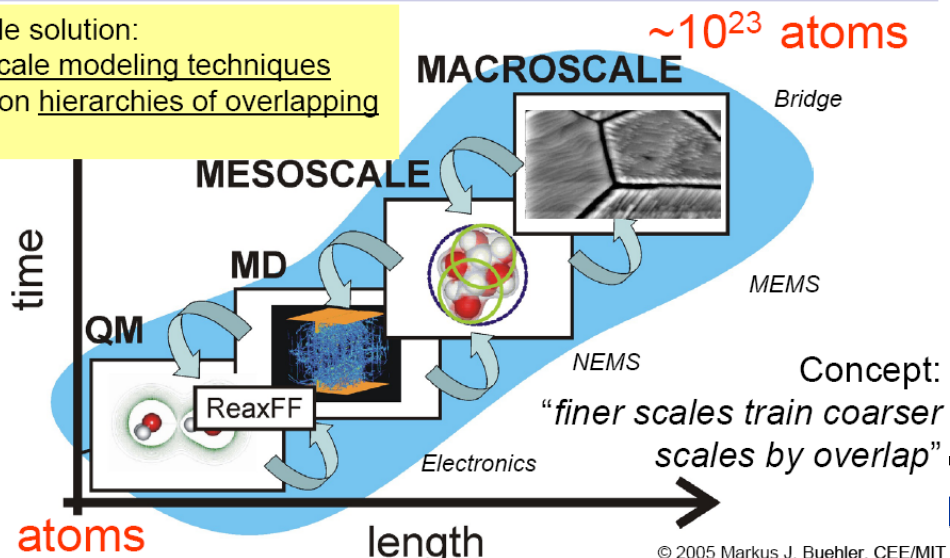

Concept:
"finer scales train coarser scales by overlap"

© 2005 Markus J. Buehler, CEE/MIT

Outline

- **Experiments and modeling of nanothermal behavior of SiC-Si_3N_4 nanocomposites with an account of hierarchy**
  - **The cohesive finite element method with focus on room temperature strength**
  - **Analyses of the effect of second phase particles and grain boundaries**
- **Analyzing superlattice interfaces for optimal thermal conduction problem in thermoelectricity**
  - **Molecular dynamic simulations to compute thermal diffusivity**
  - **Analyses of the effects of heat flow direction and grain size**
- **Achieving time-scaling by combining molecular dynamics and Monte Carlo in hybrid Monte Carlo method**
- **Designing materials in an optimization framework**
  - **A variable fidelity model management framework**

Outline

- **Experiments and modeling of nanothermal behavior of SiC-Si_3N_4 nanocomposites with an account of hierarchy**
  - **The cohesive finite element method with focus on room temperature strength**
  - **Analyses of the effect of second phase particles and grain boundaries**
- **Analyzing superlattice interfaces for optimal thermal conduction problem in thermoelectricity**
  - **Molecular dynamic simulations to compute thermal diffusivity**
  - **Analyses of the effects of heat flow direction and grain size**
- **Achieving time-scaling by combining Molecular Dynamics and Monte Carlo in Hybrid Monte Carlo Method**
- **Designing materials in an optimization framework**
  - **A variable fidelity model management framework**

Material System

- Grain boundary thickness of the order of 50 nm
- SiC particle size of the order of 200-300 nm
- Si_3N_4 grain size of the order of 0.8 to 1.5 µm
- Spherical SiC particles distributed in Si_3N_4 matrix in the form of intergranular as well as intra-granular dispersions
- SiC volume fraction varies between 10% and 50%
- Initial analyses reported here separate intra-granular, inter-granular, and mixed-granular (A combination of inter- and intra-granular) configurations with SiC volume fraction 20%

Idealized Microstructural Representation

Real Microstructure

Hypothetical Microstructure

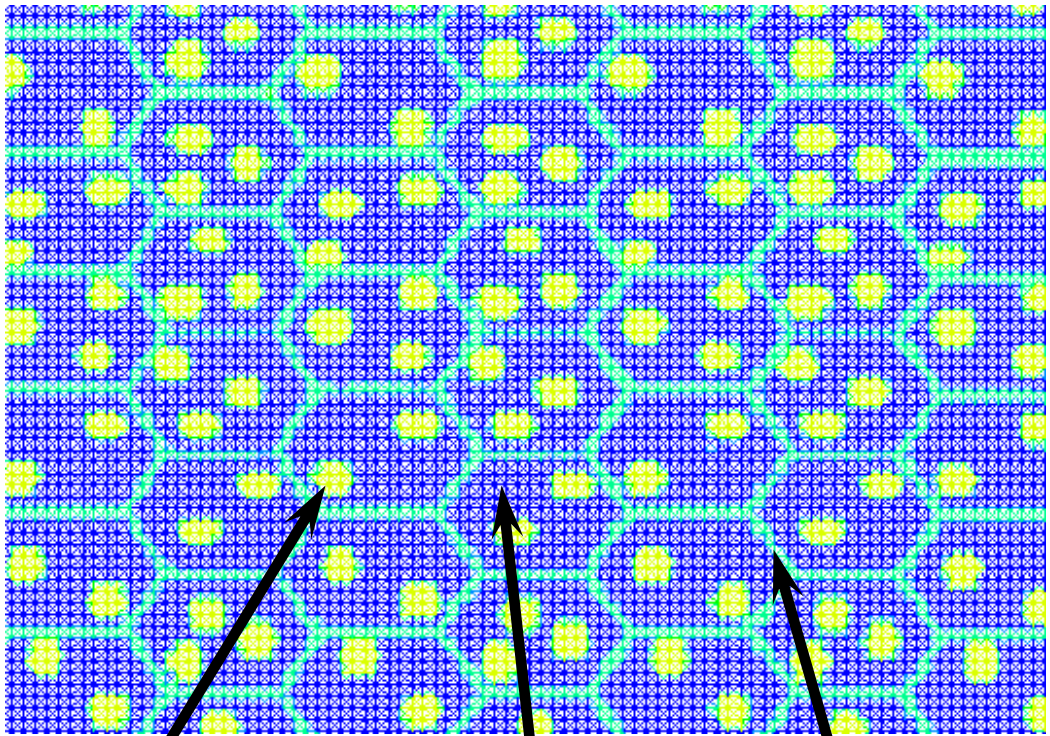

Silicon Carbide Silicon Nitride GB

AIAA, SDM-2007, Paper No. AIAA-2007-2345
Engg. Fract Mech., Mod. Sim. Mat. Sci. Engg.

Problem Setup

Total number of elements~540,000

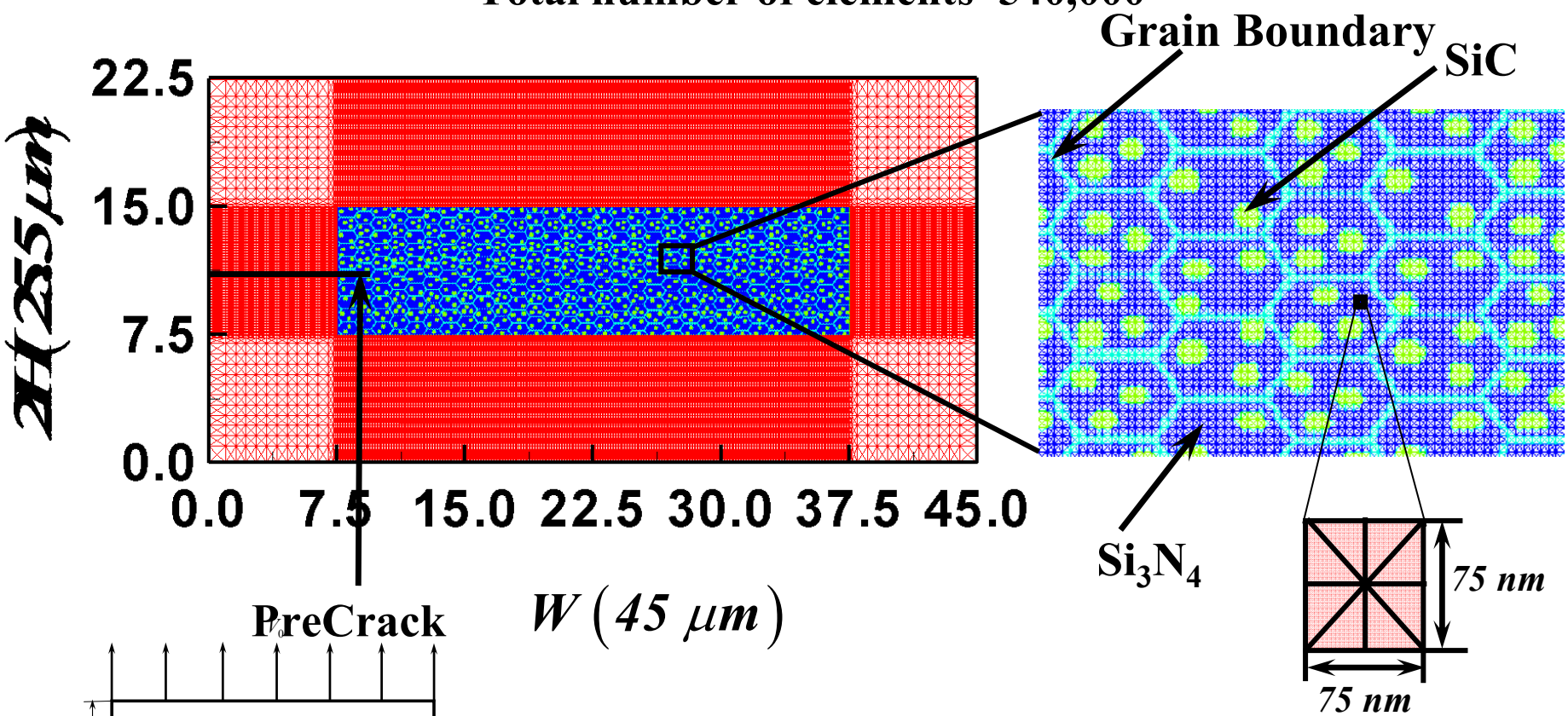

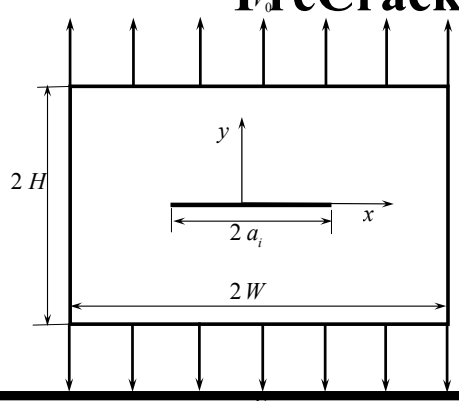

Its an image-analyses based procedure and can be easily extended to include real experimental microstructures

Microstructures of Focus-I

Class-I

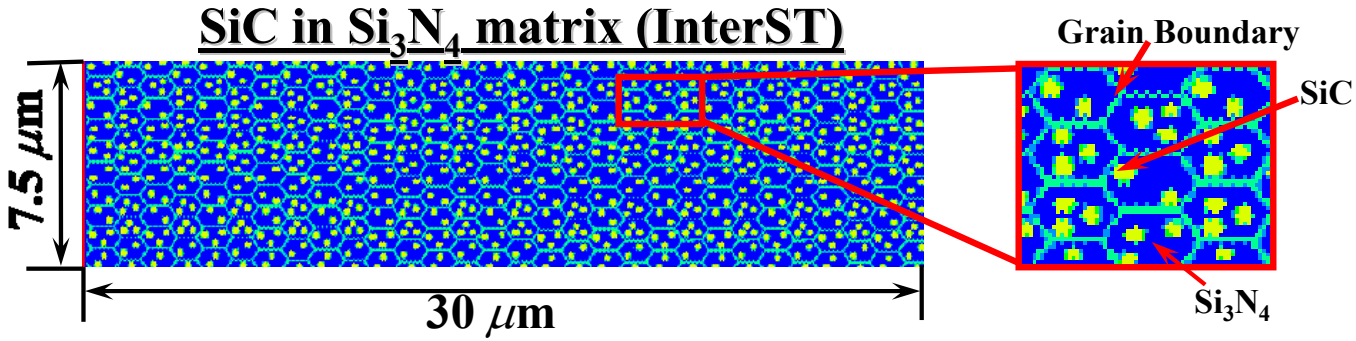

(a)

Class-II

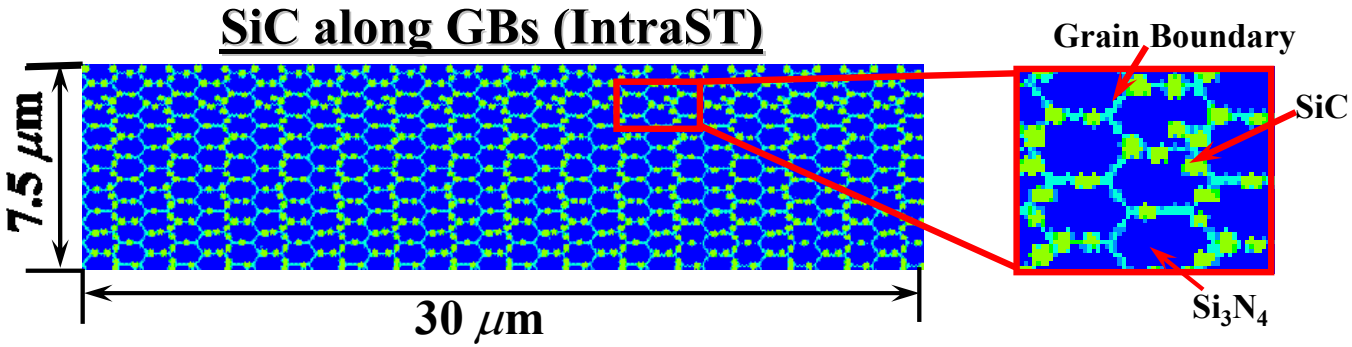

(b)

Class-III

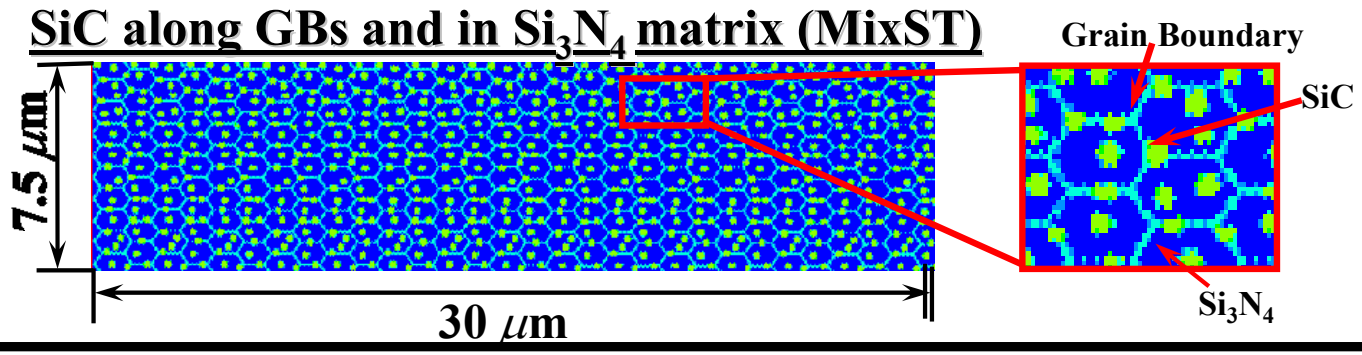

Microstructures of Focus-II

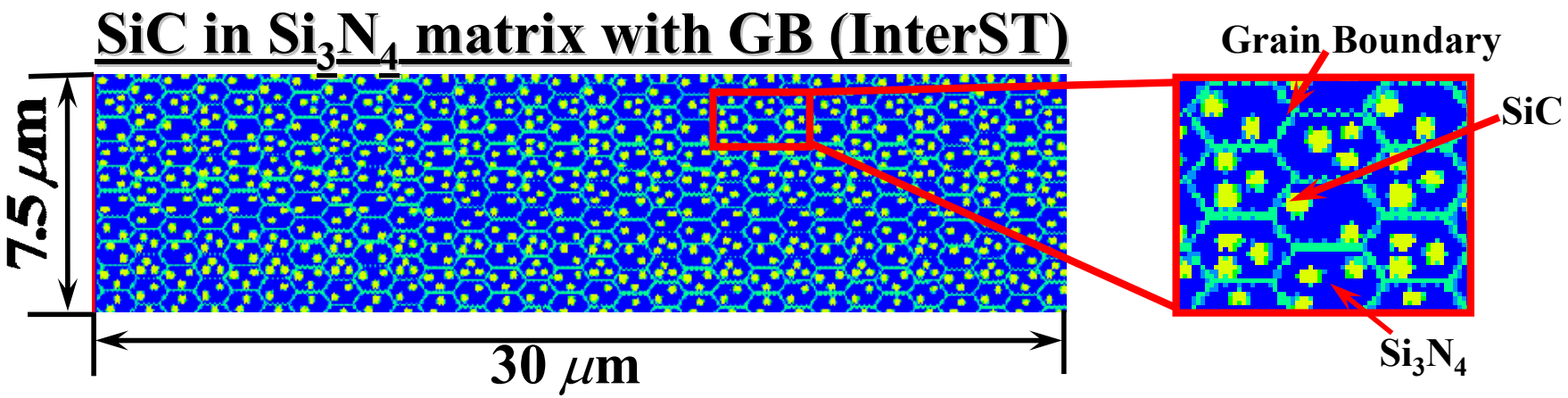

(a)

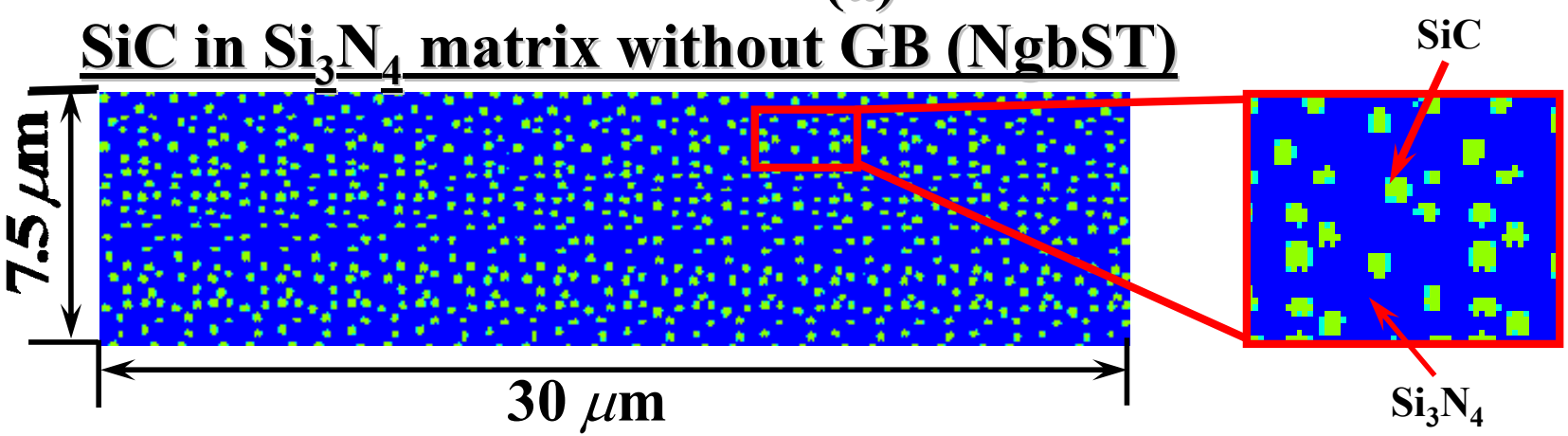

(b)

Bilinear Mixed-Mode Cohesive Law (Tomar and Zhou, 2004)

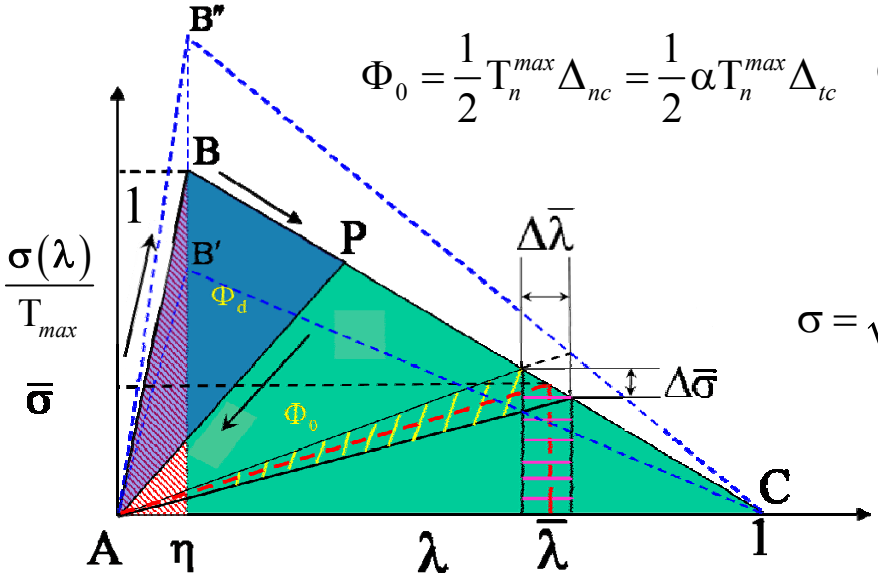

$$\Phi_0 = \frac{1}{2} T_n^{max} \Delta_{nc} = \frac{1}{2} \alpha T_n^{max} \Delta_{tc} \qquad \alpha = \Delta_{nc} / \Delta_{tc}$$

$$\sigma = \sqrt{\left(T_n\right)^2 + \left(T_t / \alpha\right)^2} = \begin{cases} \left(T_{max} \dfrac{1-\eta}{1-\eta_0}\right) \dfrac{\lambda}{\eta}, & \text{if } 0 \le \lambda \le \eta; \\ \left(T_{max} \dfrac{1-\eta}{1-\eta_0}\right) \dfrac{1-\lambda}{1-\eta}, & \text{if } \eta < \lambda \le 1; \cdot \\ 0, & \text{if } \lambda > 1. \end{cases}$$

Effective separation

$$\lambda = \sqrt{\left(\Delta_n / \Delta_{nc}\right)^2 + \left(\Delta_t / \Delta_{tc}\right)^2}$$

Effective traction

$$T_n = \sigma(\lambda, \eta) \frac{\Delta_n}{\lambda \Delta_{nc}} \quad \text{and} \quad T_t = \sigma(\lambda, \eta) \frac{\alpha \Delta_t}{\lambda \Delta_{tc}}.$$

Damage Parameter,

$$D = \frac{\Phi_d}{\Phi_0}, \qquad 0 \le D \le 1$$

Framework of Analyses

- **Bilinear Mixed-mode Cohesive law**
- **Cohesive surfaces are dispersed throughout the microstructure**
- **Bulk elemental properties are chosen to be hyperelastic considering that both SiC and Si_3N_4 are ceramics**
- **Fracture is dynamic with timestep of the velocity progression chosen based on CourantFL criterion. An additional constraint on the timestep is that the cohesive surface separation closely follows the triangular path ABC in the cohesive law**
- **Uniaxial straining NσT algorithm of Melchionna (1993 and 1995), Martyna et al. (1994) used for molecular interfacial separation analyses**
- **Minimum element size criterion and choice of meshes, (Tomar and Zhou, 2004). All cohesive properties and bulk properties chosen based on atomistic simulations satisfy the following cohesive mesh convergence criterion**

$$0.1\times\frac{9\pi E\Phi_0}{32\left(1-\nu^2\right)\mathrm{T}_{max}^2}<h<\left(\frac{\eta_0\Delta_{tc}}{\mathrm{T}_{max}}\right)\frac{E'\left(\sqrt{2}+1\right)}{(1-\nu)}.$$

Algorithm for Uniaxial Strain Deformation in MD

$$\frac{d\boldsymbol{r}(t)}{dt} = \boldsymbol{v}(t) + \eta\left(\boldsymbol{r}(t) - \boldsymbol{R}_0\right),$$

$$\frac{d\boldsymbol{v}(t)}{dt} = \frac{\boldsymbol{f}(t)}{m} - \left[\chi(t) + \eta(t)\right]\boldsymbol{v}(t),$$

$$\frac{d\chi(t)}{dt} = \frac{2E_{kin}(t) - 2\sigma - 3^2 k_B T_{ext}}{q_{mass}},$$

$$q_{mass} = 2\sigma\tau_T^2$$

$$\frac{d\boldsymbol{\eta}(t)}{dt} = \frac{\left(\boldsymbol{\sigma}(t) - \boldsymbol{\sigma}_{ext}\right)V(t)}{p_{mass}} - \chi(t)\boldsymbol{\eta}(t)$$

$$p_{mass} = \frac{(f+3)}{3} k_B T_{ext} \tau_P^2$$

$$\frac{d\boldsymbol{H}(t)}{dt} = \boldsymbol{\eta}(t) \cdot \boldsymbol{H}(t)$$

$$\frac{dV(t)}{dt} = Tr\left[\boldsymbol{\eta}(t)\right]V(t),$$

- **Melchionna (1993 and 1995), Martyna et al. (1994) NσT algorithm (recently used with HMC in Tomar, 2007, JAP and Physica Status Solidi-a)**
- **Of all the quantities η_{11} determines the stretch of cell along x-axis**
- **At each time-step σ_{ext} adjusted such that η_{11} value results in stretching of cell at the specified strain rate for example at an instantaneous cell length, η_{11}=0.0001 corresponds to a strain rate of 10^8 s^{-1}**
- **Three combinations of τ_T and τ_P are tried (0.15:1.25, 0.25:1.5, and 1.5:2.0) and 0.25:1.5 chosen for least fluctuations in pressure and conserved quantity (Gibbs Energy)**
- **Stress calculated correspond to true stress and strain correspondingly to true strain**

Atomistic Deformation

SiC-SiC (Tersoff Potential, 1988))

Si_3N_4-Si_3N_4 (Gale Potential, 2001)

For SiC-Si_3N_4 A combination of Tersoff, Garofelini potentials with first principle calculation derived C-N bond energies

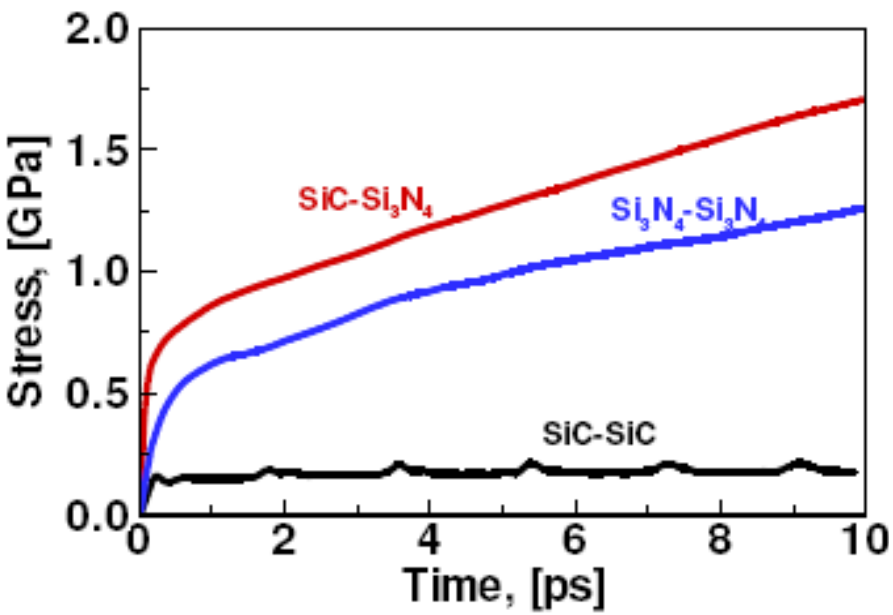

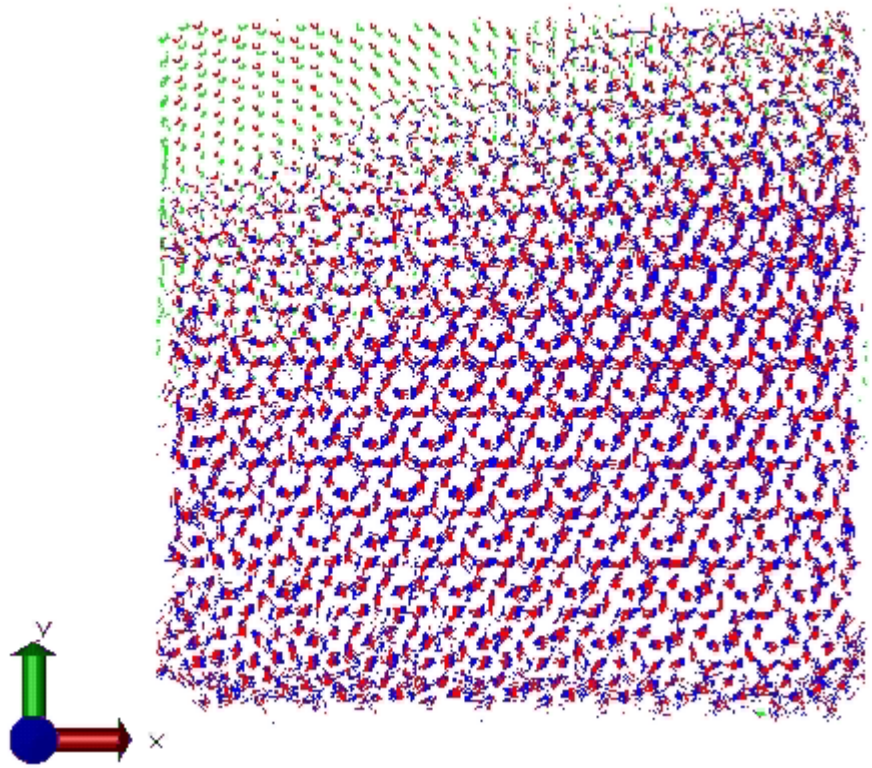

The cohesive traction value motivated from peak separation strength in the atomistic simulations

Framework of Analyses: Material Properties with GBs

Component	Φ (N/m)	T (GPa)	Δ_c (nm)	E (GPa)	ν	ρ (kg/m^3)
SiC (sc)	19.53	1.02	38.3	449	0.16	3215
Si_3N_4 (sn)	191.5	2.3	166.5	210	0.22	2770
GBs (g)	238.7	2.38	200.6	200	0.16	4000
(sc-g)	19.53	1.02	38.3	--	--	--
(sc-sn)	19.53	1.02	38.3	--	--	--
(sn-g)	191.5	2.3	166.5	--	--	--
Homogenized (H)	127.8	2.03	125.9	256.8	0.202	2982
H-sc	19.53	1.02	38.3	--	--	--
H-sn	127.8	2.03	125.9	--	--	--
H-gb	127.8	2.03	125.9	--	--	--

Damaging Effect of Second Phase Particles

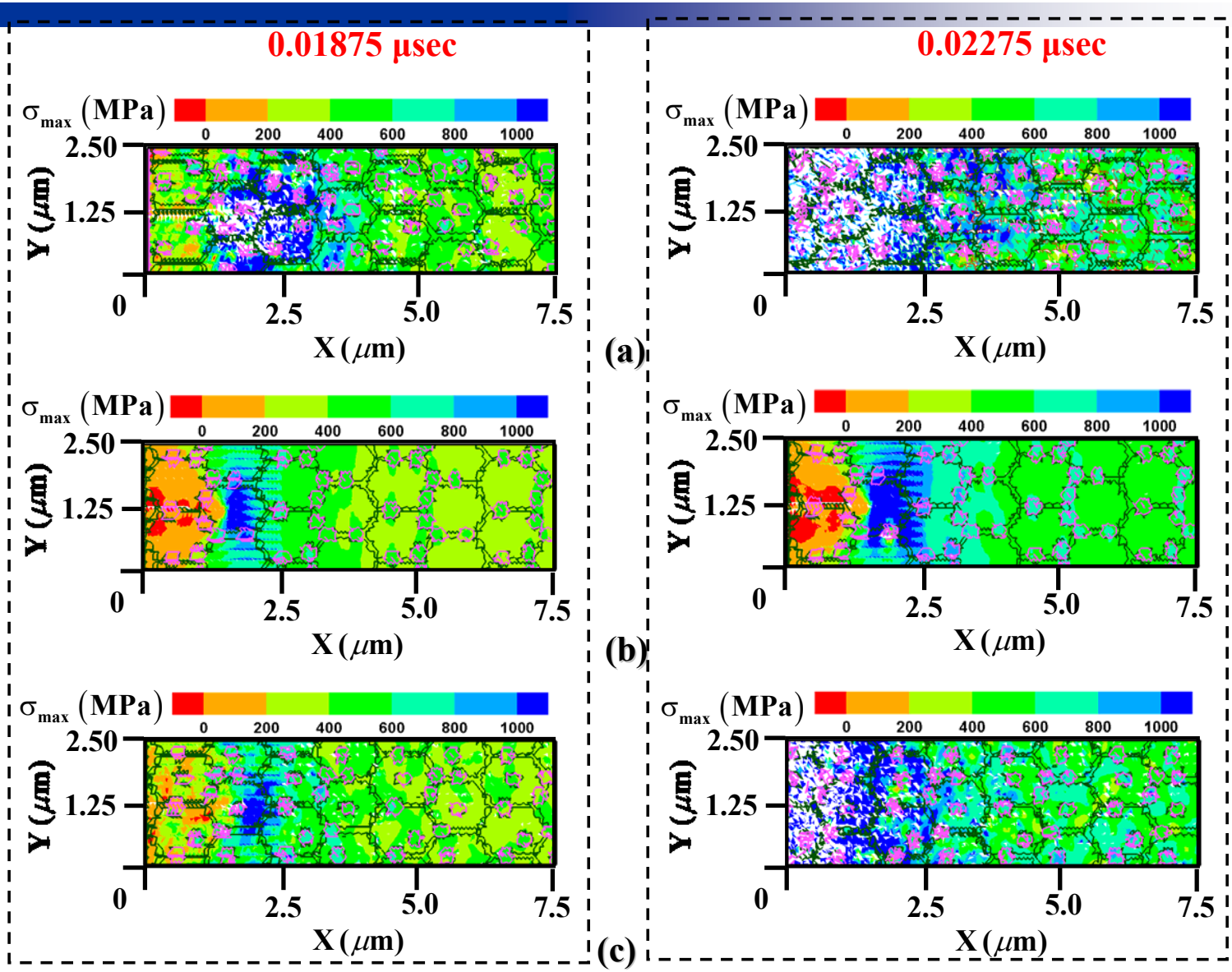

Damaging Effect of GBs

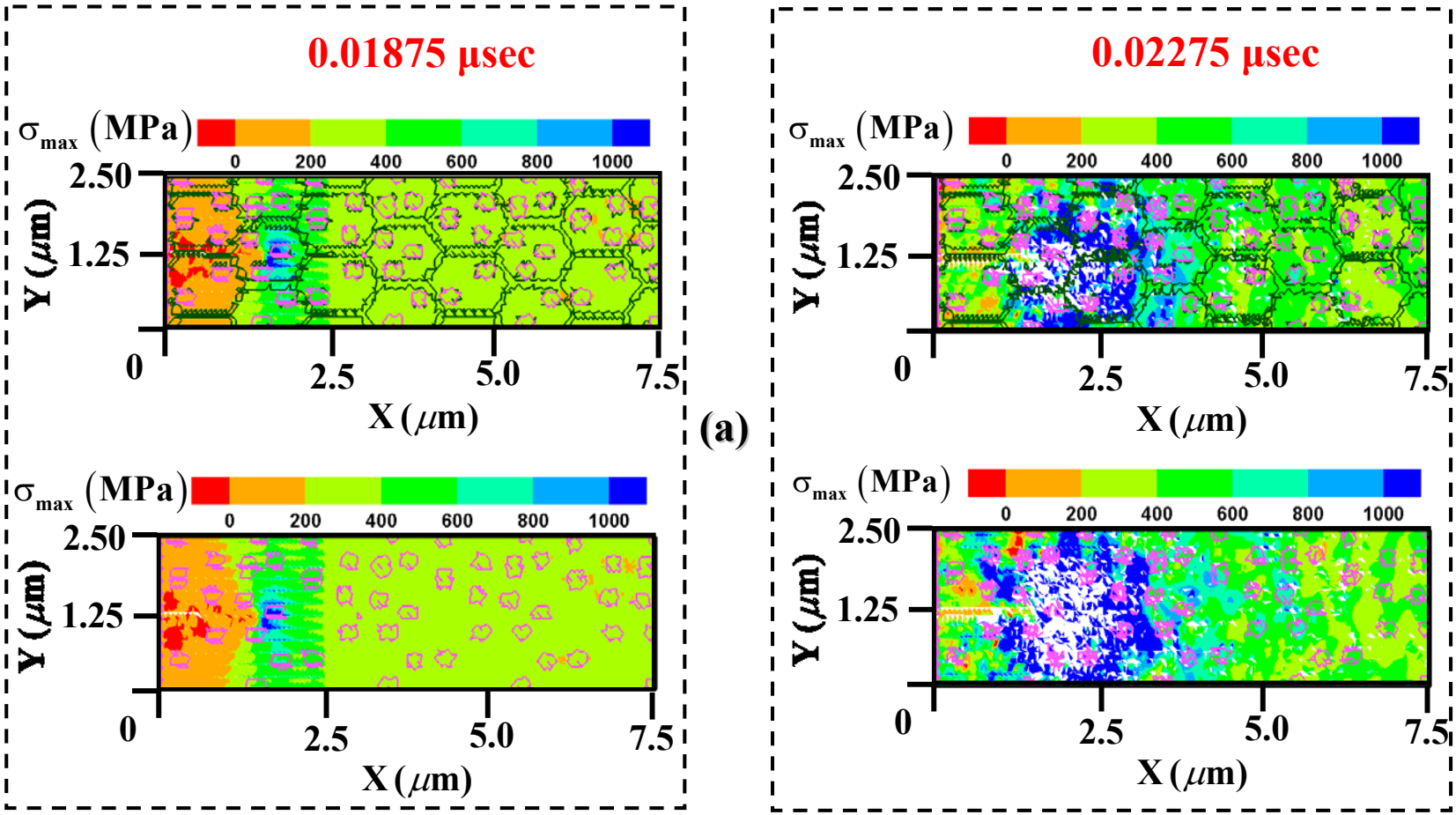

Second Phase Particles Effect on Crack Density

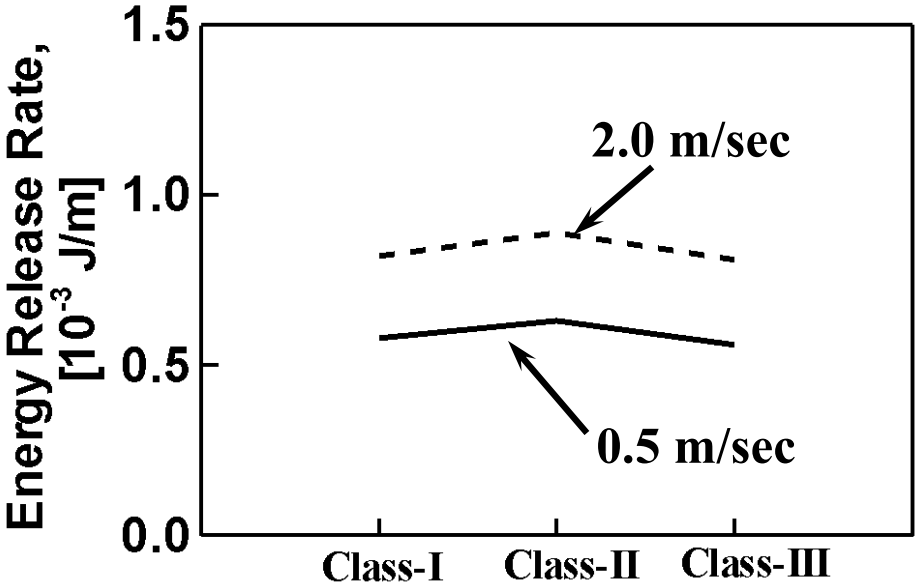

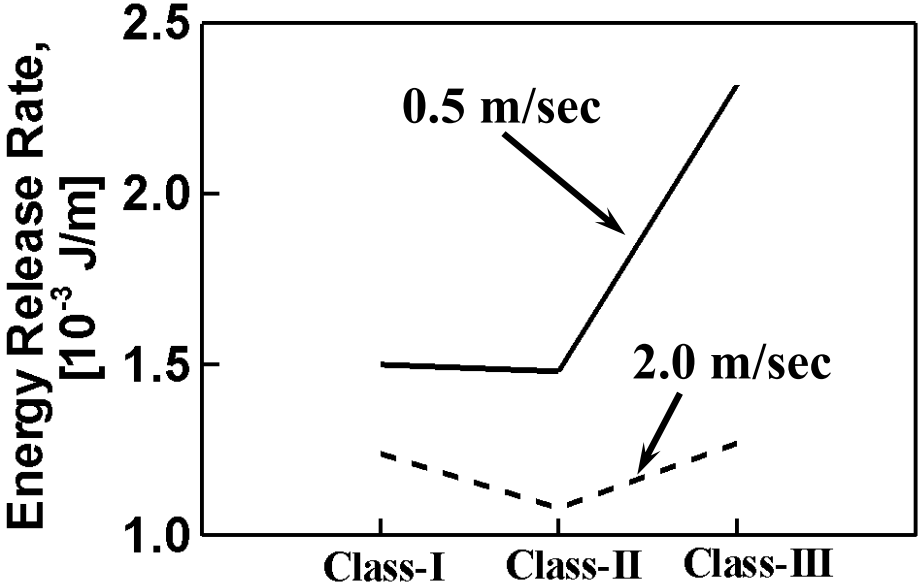

- Higher second phase particle numbers in the matrix directly relate to higher crack density
- In some cases second phase particles in matrix act to bridge the cracks leading to lowering of crack density

GB Effect on Crack Density

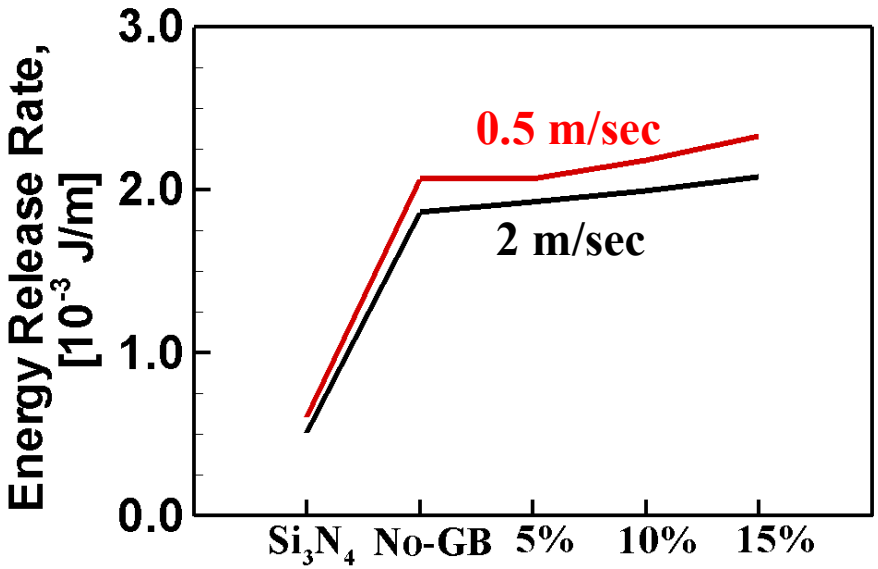

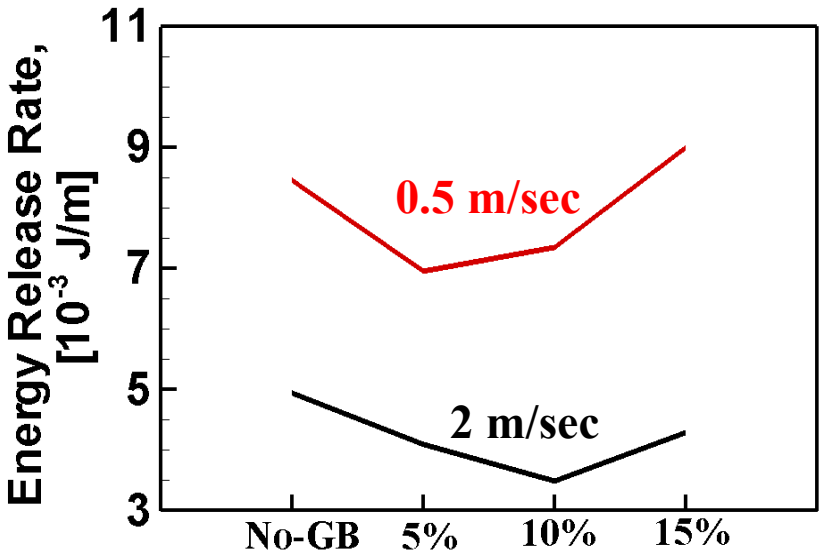

- GBs tend to limit the damage
- Least damaged microstructure is the one with second phase particles lying along-side GBs in the matrix acting as crack bridging elements

$SiC\text{-}Si_3N_4$ Nanocomposites: High Temperature Constitutive Model

$$\sigma = \sigma_0 \left[1 + \left(\frac{\varepsilon}{\varepsilon_0} \right)^n \right] \left[\frac{\dot{\varepsilon}}{\dot{\varepsilon}_0} \cdot \exp\left(\frac{Q}{RT} \right) \right]^m$$

Rouxel and Besson, 1997

Lei, Shin, Incropera, 2000

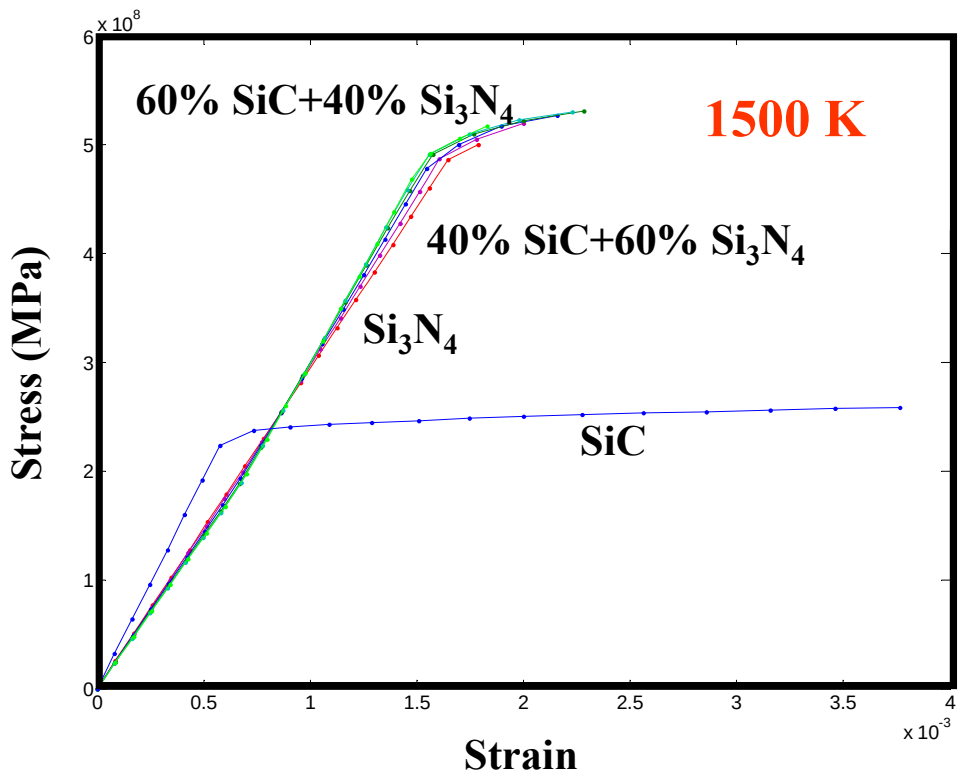

Cohesive Model of Intergranular Glass Phase

$$\lambda = \left[\left(\frac{\delta_n}{\delta_{n\,\max}} \right)^2 + \left(\frac{\delta_t}{\delta_{t\,\max}} \right)^2 \right]^{1/2} \quad \text{for tensile loading } (\delta_n \geqslant 0)$$

$$F(\lambda) = \frac{27}{4} t_{n0}(T)(1-\lambda)^2 \quad \text{for } 0 \leqslant \lambda \leqslant 1$$

$$t_n = \frac{\delta_n}{\delta_{n\,\max}} F(\lambda_{\max}) \qquad t_t = \alpha \frac{\delta_t}{\delta_{t\,\max}} F(\lambda_{\max})$$

$$G_c = \int_0^{\delta_{\max}} t\,d\delta = \int_0^{\delta_{\max}} \frac{27}{4} t_0 \frac{\delta}{\delta_{\max}} \left(1 - \frac{\delta}{\delta_{\max}}\right)^2 d\delta = \frac{27}{48} t_0 \delta_{\max}$$

$$G_C = \frac{K_C^2(1-\nu)}{E}$$

$$t_{n0}(T) = t_0 \left[\frac{Q}{RT} - \ln(k_t \cdot t_F) \right]$$

$$\mathbf{D} = \frac{\partial \mathbf{t}}{\partial \boldsymbol{\delta}} = \begin{bmatrix} \frac{\partial t_n}{\partial \delta_n} & \frac{\partial t_n}{\partial \delta_t} \\ \frac{\partial t_t}{\partial \delta_n} & \frac{\partial t_t}{\partial \delta_t} \end{bmatrix}$$

$$\mathbf{F} = \int \mathbf{N}^T \cdot \mathbf{t}\,dA \qquad \mathbf{K} = \int (\mathbf{N}^T \cdot \mathbf{D} \cdot \mathbf{N})\,dA$$

In ABAQUS, the cohesive element is defined through a user defined subroutine.

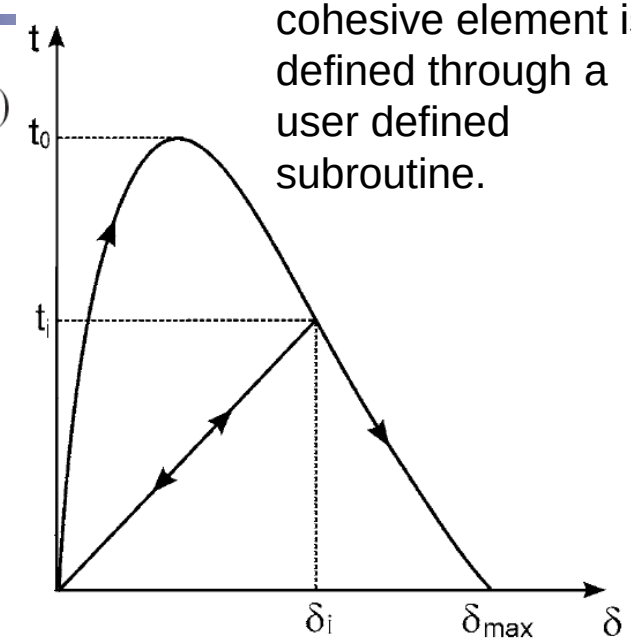

Sketch of an irreversible cohesive model.

G_C = fracture energy, J

λ = cohesive damage parameter

δ_n = normal opening displacement of a cohesive pair, m

δ_t = tangential opening displacement of a cohesive pair, m

t = cohesive stress, MPa

t_{n0} = normal strength of a cohesive pair, N

t_{t0} = tangential strength of a cohesive pair, N

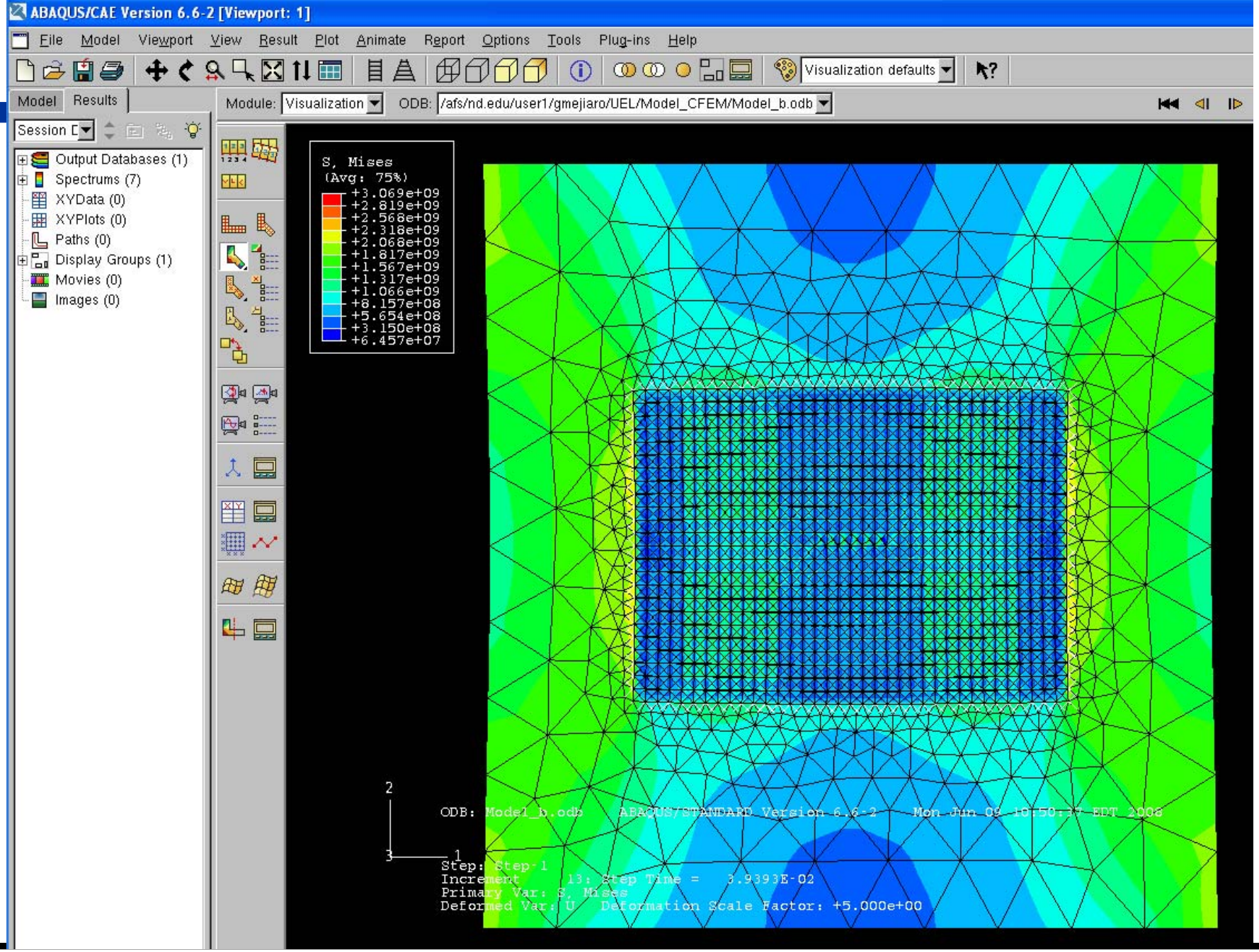
ABAQUS/CAE Version 6.6-2 [Viewport: 1]
File Model Viewport View Result Plot Animate Report Options Tools Plug-ins Help
Visualization defaults
Model Results
Module: Visualization
ODB: /afs/nd.edu/user1/gmejiaro/UEL/Model_CFEM/Model_b.odb
Output Databases (1)
Spectrums (7)
XYData (0)
XYPlots (0)
Paths (0)
Display Groups (1)
Movies (0)
Images (0)
S, Mises
(Avg: 75%)
+3.069e+09
+2.819e+09
+2.568e+09
+2.318e+09
+2.068e+09
+1.817e+09
+1.567e+09
+1.317e+09
+1.066e+09
+8.157e+08
+5.654e+08
+3.150e+08
+6.457e+07
ODB: Model_b.odb ABAQUS/STANDARD Version 6.6-2 Mon Jun 09 10:50:17 EDT 2008
Step: Step-1
Increment 13: Step Time = 3.9393E-02
Primary Var: S, Mises
Deformed Var: U Deformation Scale Factor: +5.000e+00

Experimental Investigations

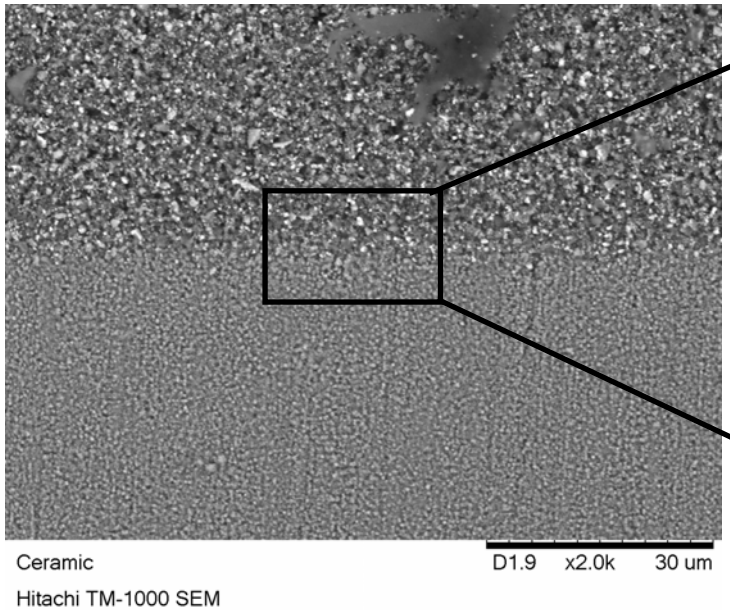

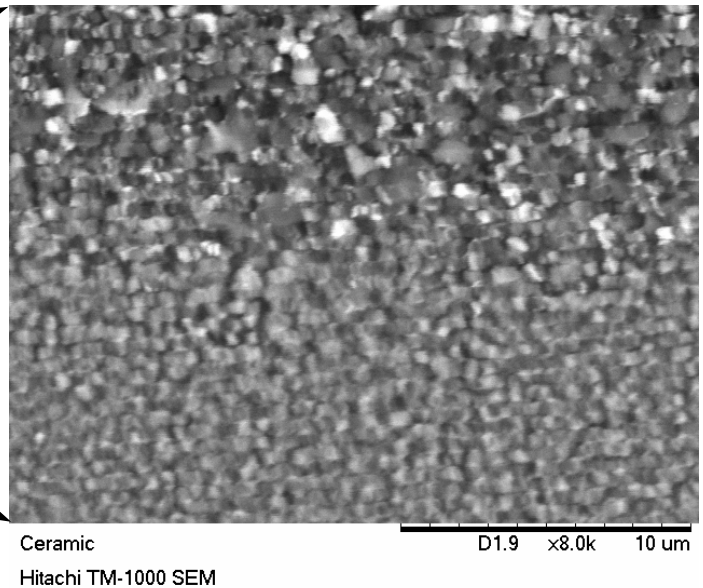

Nanoindentation

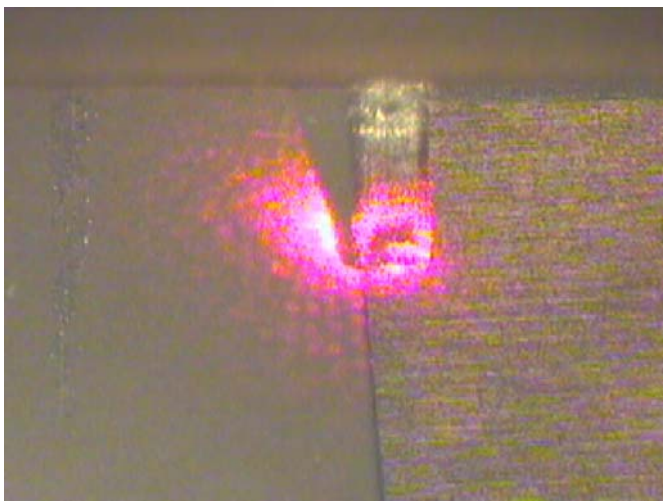

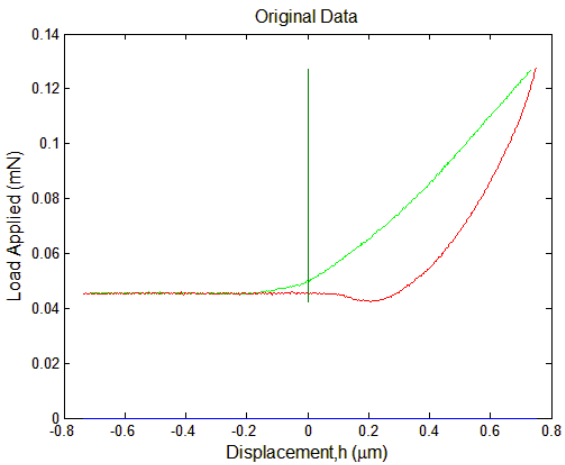

Conclusions and Summary

- A method for analyzing dynamic fracture in SiC-Si_3N_4 nanocomposites with molecular motivated interfacial separation laws is presented
- Preliminary interfacial laws are motivated from a single set of molecular interfacial separation analyses and experimental observations
- Analyses are performed on a range of inter-, intra-, and mixed granular nanocomposite configurations
- Analyses clearly establish the dominant role played by the grain boundaries in and the second phase particles in the fracture strength of this important class of nanocomposites
- New directions include nanomechanical testing and Abaqus implementation of high temperature cohesive testing

DE-FG26-07NT43072: Program Manager Dr. Patricia Rawls

Outline

- Experiments and modeling of nanothermal behavior of SiC-Si_3N_4 nanocomposites with an account of hierarchy
  - The cohesive finite element method with focus on room temperature strength
  - Analyses of the effect of second phase particles and grain boundaries
- **Analyzing superlattice interfaces for optimal thermal conduction problem in thermoelectricity**
  - **Molecular dynamic simulations to compute thermal diffusivity**
  - **Analyses of the effects of heat flow direction and grain size**
- Achieving time-scaling by combining Molecular Dynamics and Monte Carlo in Hybrid Monte Carlo Method
- Designing materials in an optimization framework
  - A variable fidelity model management framework

Macroscale → Nanoscale

Nanoscale thermal transport is important when either the individual energy carriers must be considered and/or when continuum models break down.

Bulk

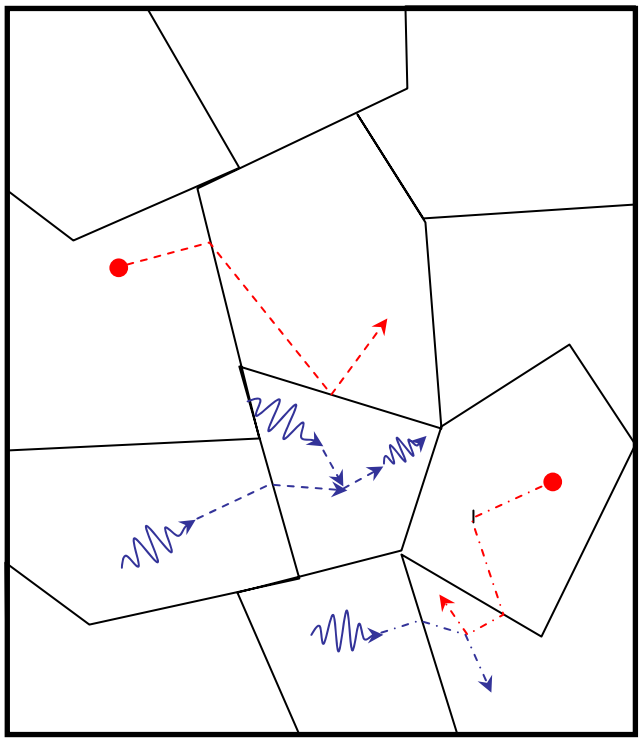

$$\frac{\partial}{\partial x}\left(k_x \frac{\partial T}{\partial x}\right)+\frac{\partial}{\partial y}\left(k_y \frac{\partial T}{\partial y}\right)+\frac{\partial}{\partial z}\left(k_z \frac{\partial T}{\partial z}\right)+\dot{q}=\rho c_p \frac{\partial T}{\partial t}$$

Nanostructure

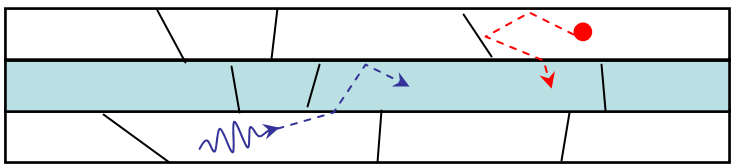

Si/Ge Superlattice

- Drastic drop in thermal conductivity for L>130Å was explained with the concept of critical thickness(h_c) for the formation of dislocations. For Si/Ge, L>130Å, the Si layers have greatly exceeded h_c and introduces a large density of dislocations and stacking faults.
- Else, the general trend to be found was increase in k with increase in period thickness of the superlattice.
- Diffuse Mismatch Model (DMM) failed to explain the behavior and under-predicted the k values by factor of 3-8.

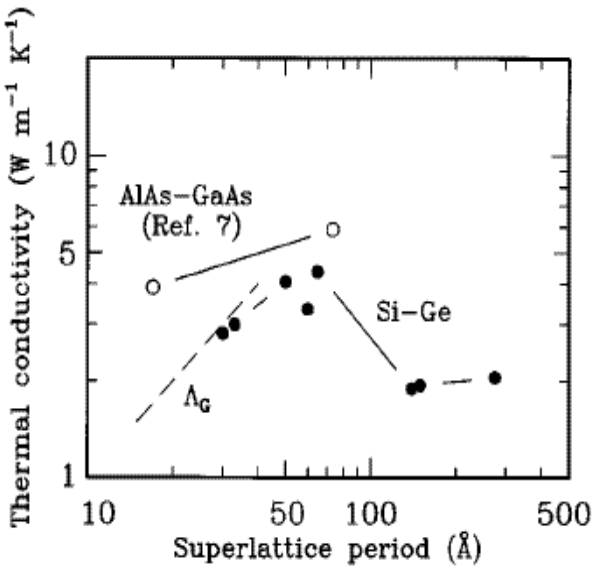

Fig: Thermal conductivity of Si-Ge superlattices at 200K plotted as a function of Superlattice period L

NEMD: Methodology

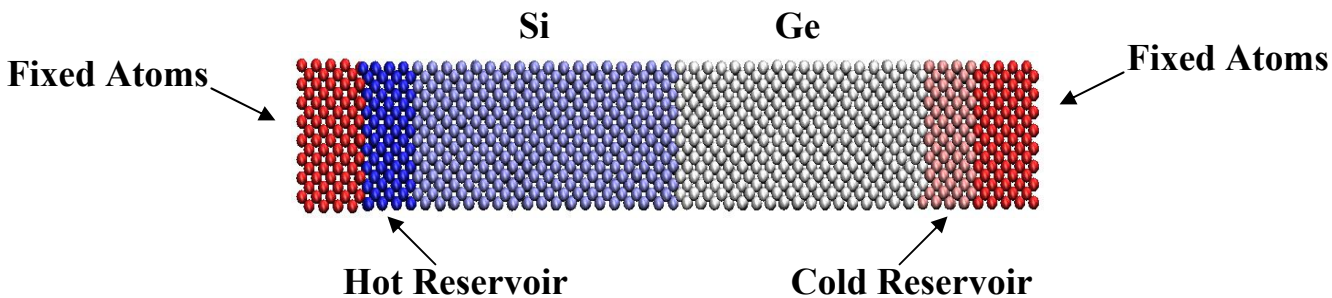

- **Two layers of 10A^0 thickness which is around 4 atomic layer are placed at the two ends and are kept at zero velocity throughout the simulation to simulate the Thin Film Superlattice structure.**

- **The layers marked '*Hot Reservoir*' and '*Cold Reservoir*', adjacent to Fixed atomic layers are kept at Constant temperature throughout the simulation by rescaling the velocities at every time step using the *"Constant temperature gradient and momentum conserved method (CTGMC)"* proposed by *Mountain et al.***

Ref: R.D. Mountain, R.A. MacDonald , Phys. Rev. B 28 (1983) 3022.

Terminology

$(5_{Si}\times5_{Ge})_1$: One Period of 5 nm Si & 5 nm Ge

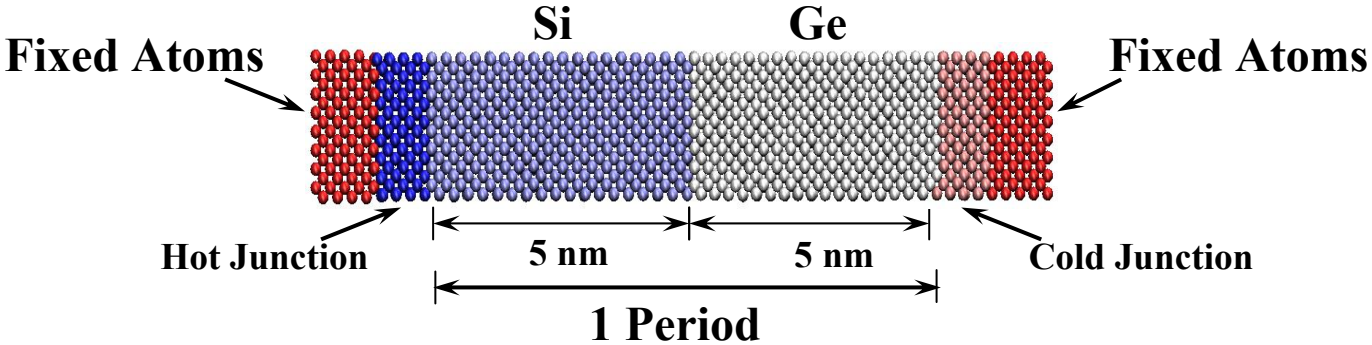

(a)

$(5_{Si}\times5_{Ge})_3$: Three Periods of 5 nm Si & 5 nm Ge

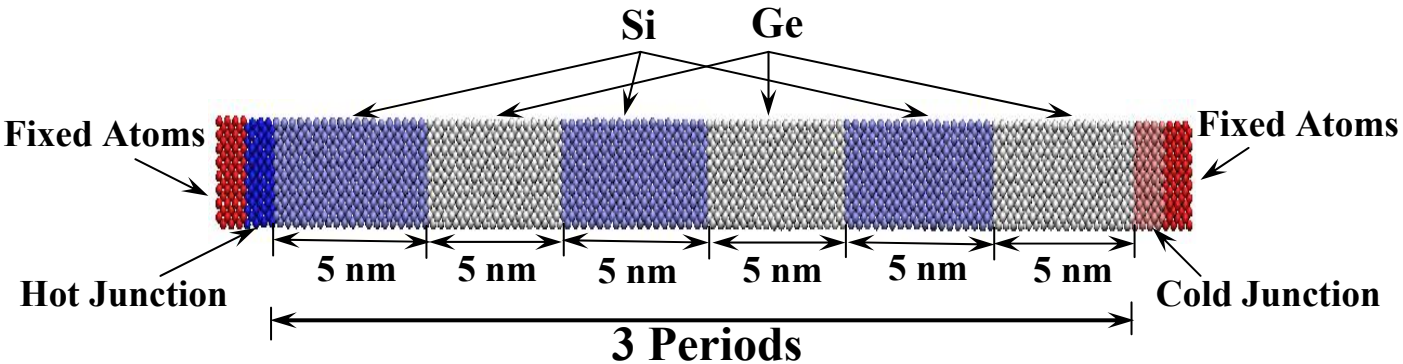

(b)

Temperature Profile along Length of Superlattice

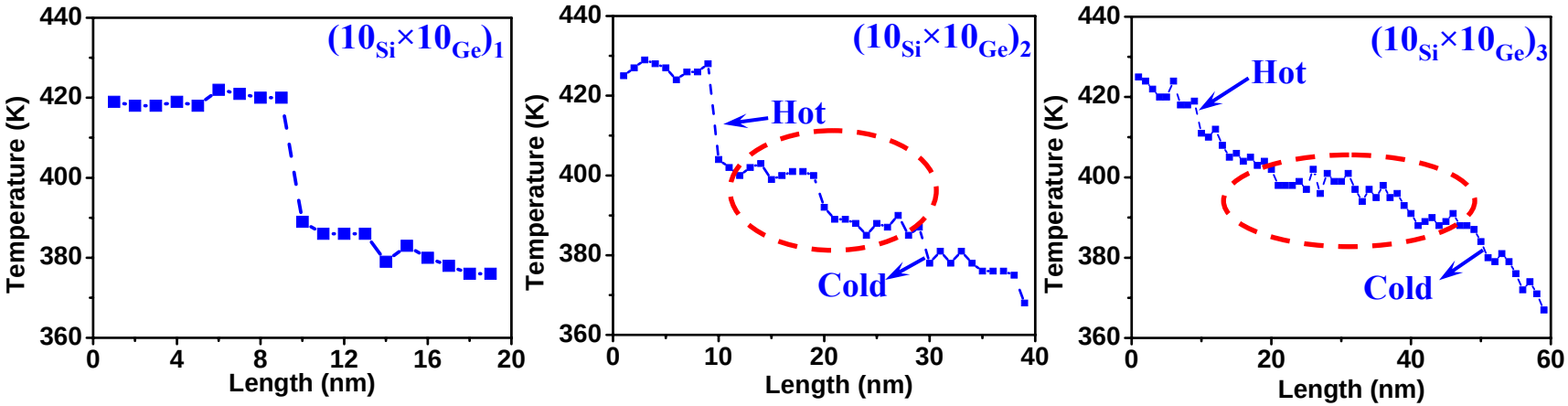

- The drop in the temperature at the interface is attributed to thermal boundary resistance
- As the number of Layers increase, the individual resistance of a solid-solid interface to thermal transport seems to vary along the length of the system.
- Temperature Drop, $\Delta T = f(T, L, period, position)$

Samvedi & Tomar, Submitted PRB and JAP

Thermal Boundary Resistance

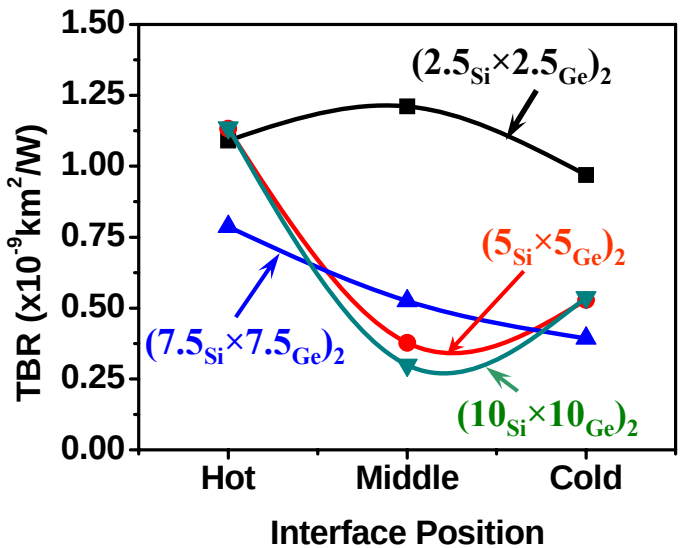

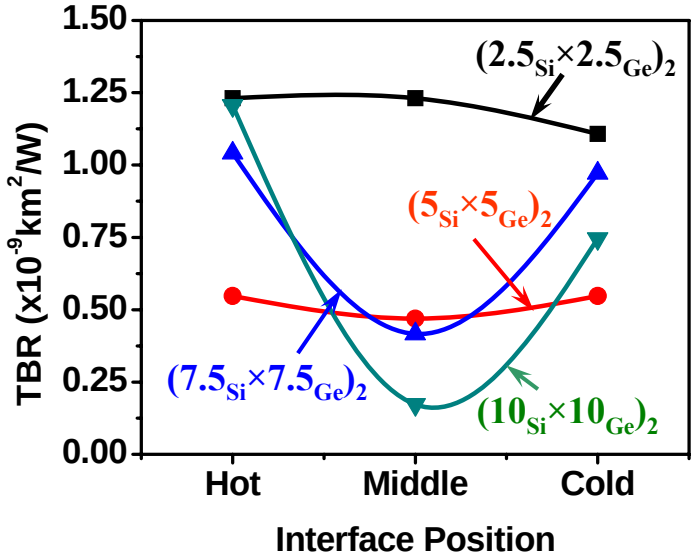

- **TBR at a particular solid-solid interface not only depends on the Acoustic Mismatch across the interface, but also on the location of the interface in a superlattice system.**
- **Trend in the variation of TBR depends both on Temperature as well as Period thickness.**

Thermal Boundary Resistance Expression

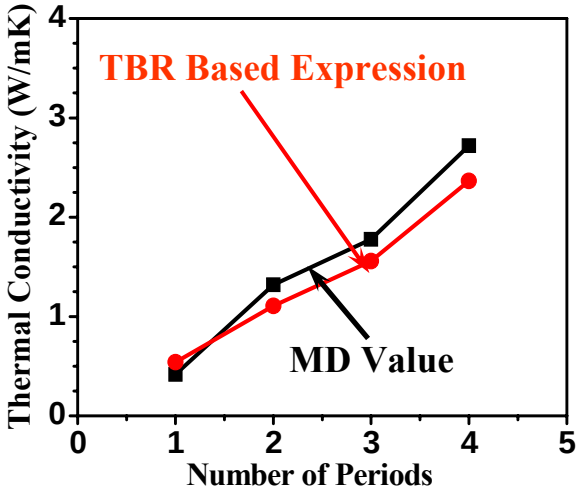

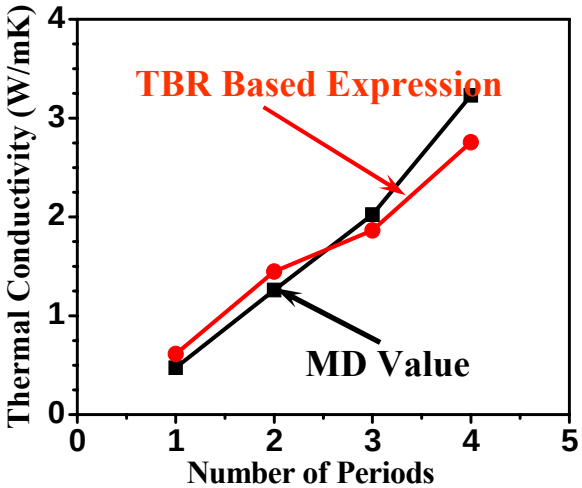

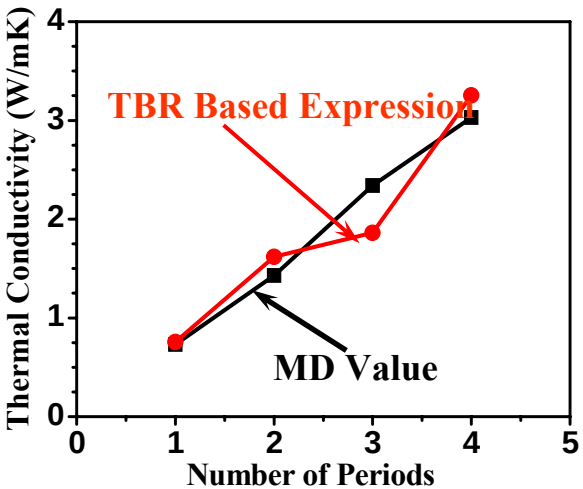

$$k^{-1} = \frac{\sum_i L_{Si}}{L_z} k_{Si}^{-1} + \frac{\sum_i L_{Ge}}{L_z} k_{Ge}^{-1} + \frac{R_{BD}}{L_z}.$$

Heat Flow Direction : Si/Ge vs. Ge/Si

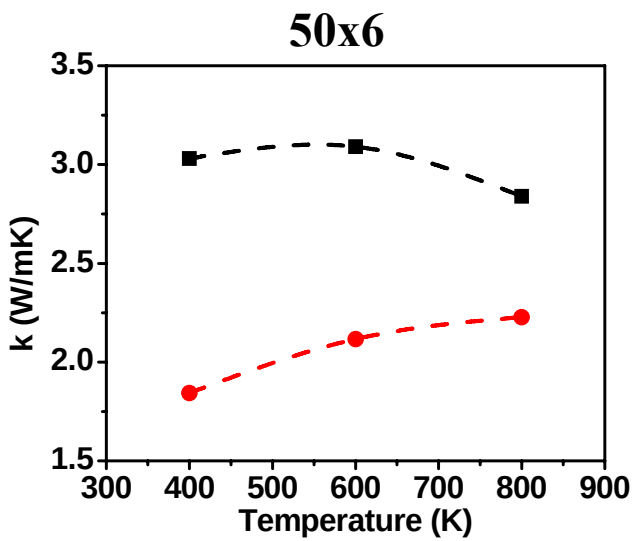

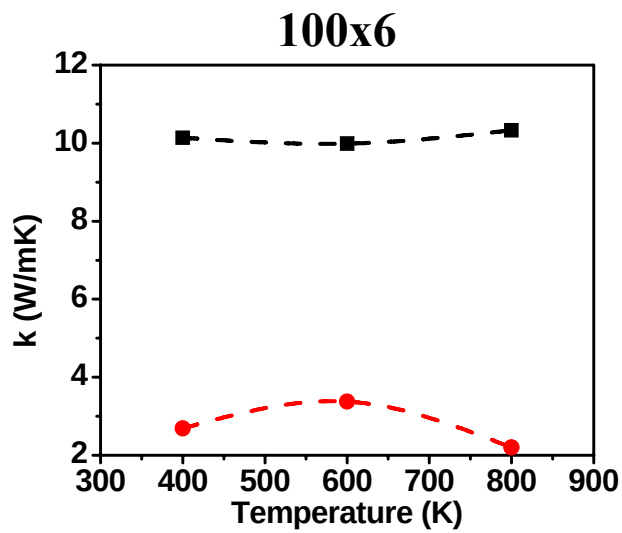

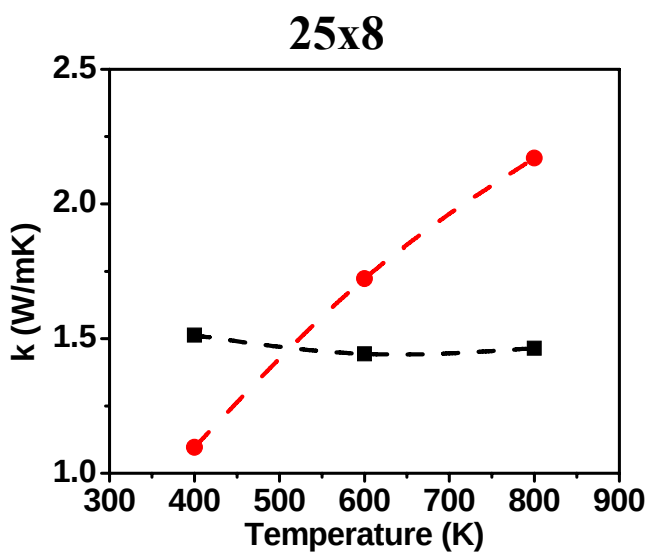

- Thermal Conductivity difference between two systems, with heat flow in opposite directions depends both on the period and number of interfaces.
- Difference depends strongly on the number of layers, i.e. number of interfaces encountered and not very significantly on the period of the superlattice.

$SiC\text{-}Si_3N_4$ Nanocomposites

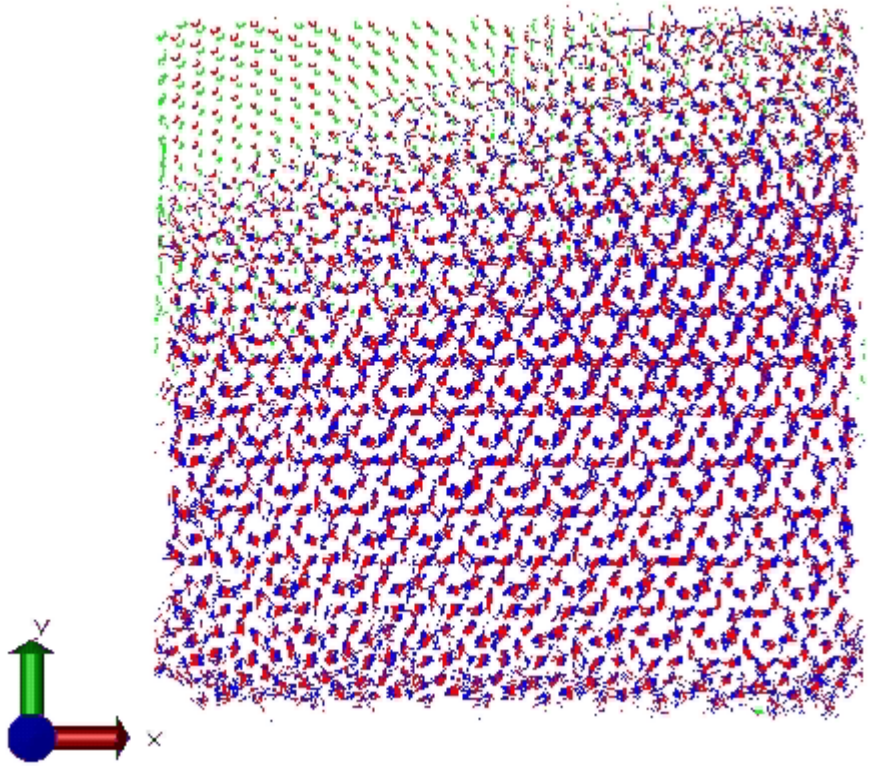

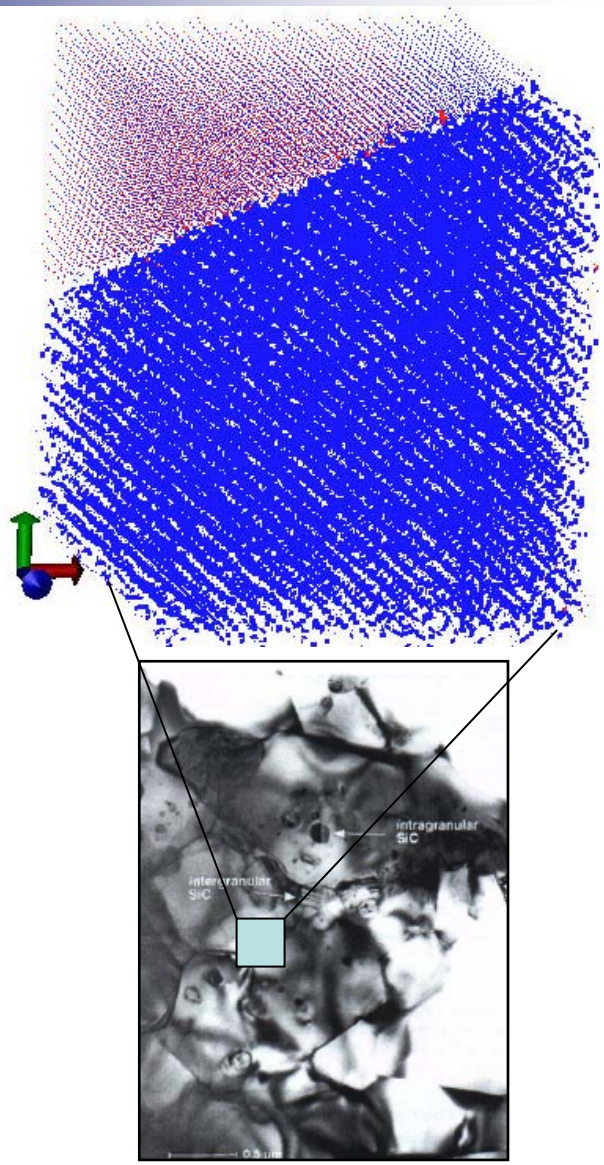

$SiC-Si_3N_4$ Nanocomposites: Thermal Conductivity Comparisons

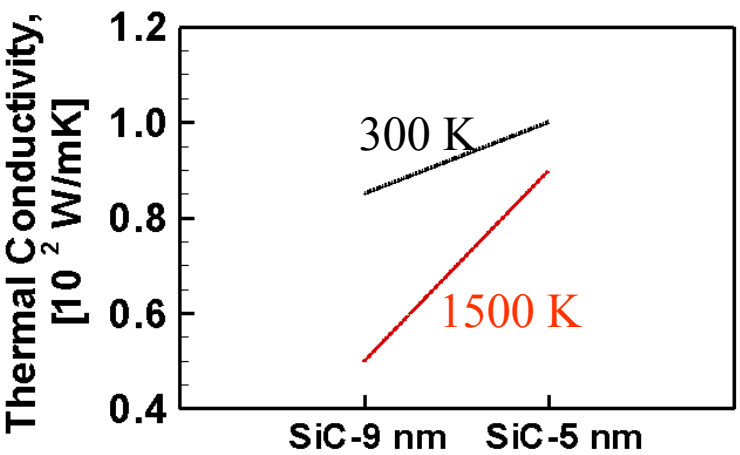

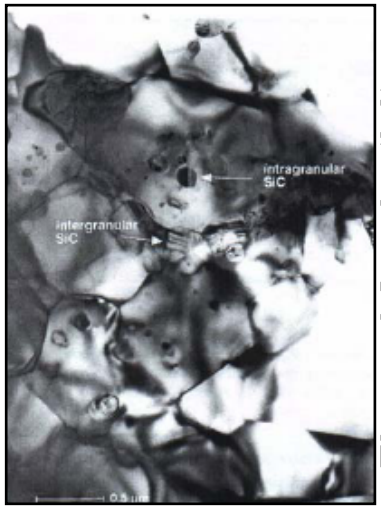

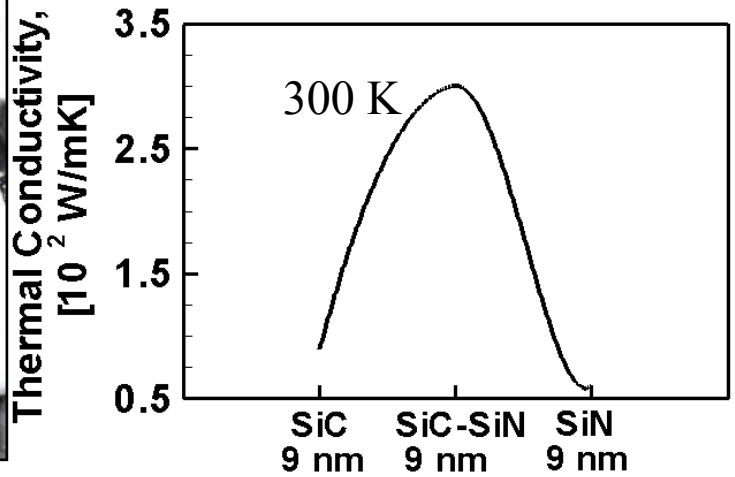

Conclusion

- Thermal conductivity of Si-Ge super-lattice and SiC-Si_3N_4 nanocomposite interfaces analyzed
- Applied strain can significantly reverse the usual thermal conductivity picture
- Superlattice period is an important parameter to control thermal conductivity
- Thermal boundary resistance can be tailored better by doping in the middle layers
- Thermal conductivity is also dependent upon the direction of measurement
- Non-traditional interfaces can significantly increase the thermal conductivity

DE-FG26-07NT43072: Program Manager Dr. Patricia Rawls

Outline

- Experiments and modeling of nanothermal behavior of SiC-Si_3N_4 nanocomposites with an account of hierarchy
  - The cohesive finite element method with focus on room temperature strength
  - Analyses of the effect of second phase particles and grain boundaries
- Analyzing superlattice interfaces for optimal thermal conduction problem in thermoelectricity
  - Molecular dynamic simulations to compute thermal diffusivity
  - Analyses of the effects of heat flow direction and grain size
- **Achieving time-scaling by combining Molecular Dynamics and Monte Carlo in Hybrid Monte Carlo Method**
- Designing materials in an optimization framework
  - A variable fidelity model management framework

Hybrid Monte Carlo Method for Timescaling

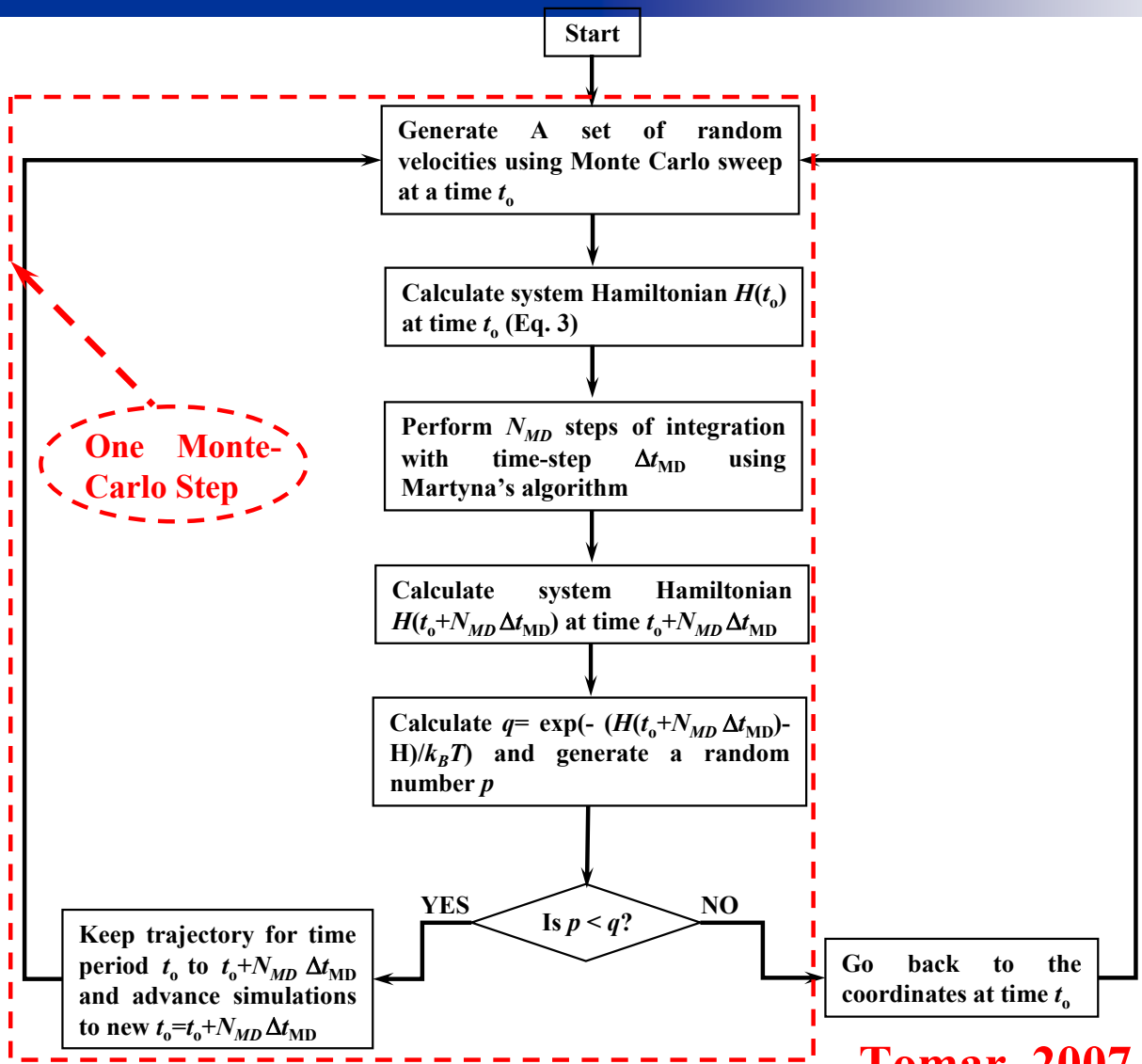

Tomar, 2007, JAP and PSSA

HMC Nanowire: Δt=8 fs N_{MD}=2, 8, 32

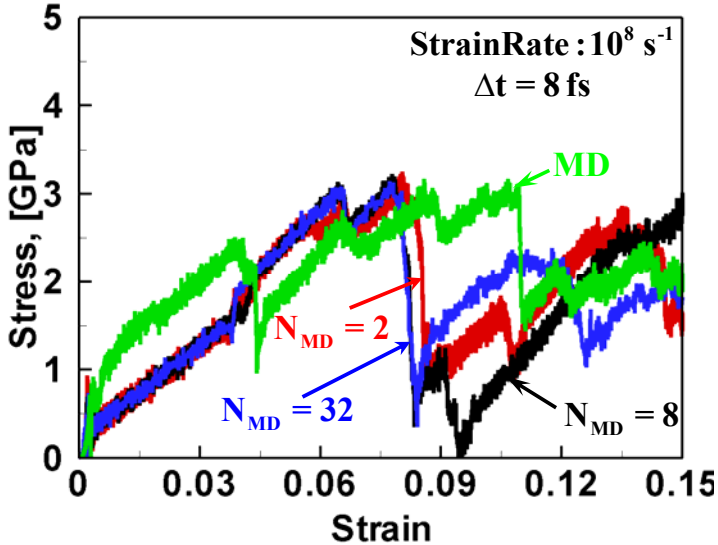

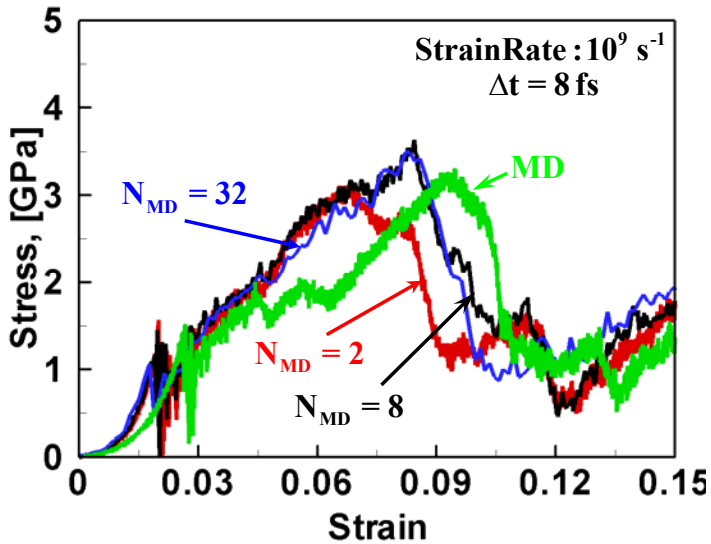

10^9 s^{-1}

HMC Δt=8 fs N_{MD}=8 **MD Δt=2 fs**

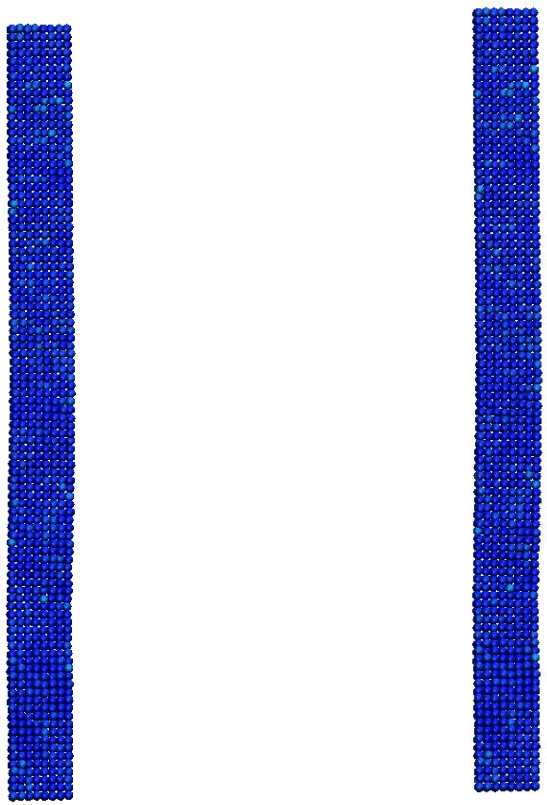

HMC Nanocrystalline Ni: Δt=8 fs N_{MD}=2, 8, 32

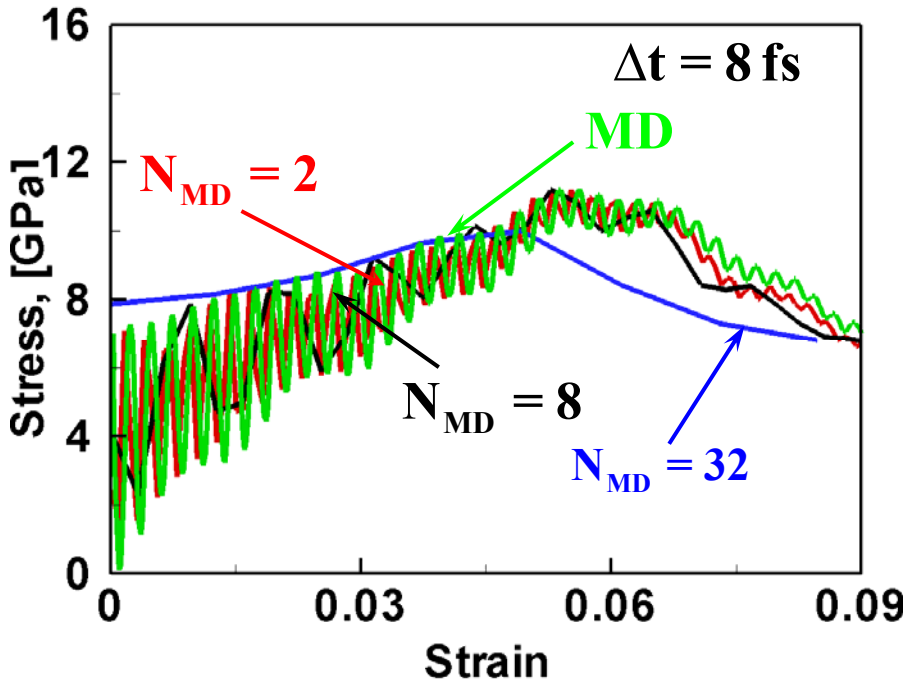

MD Δt=2 fs

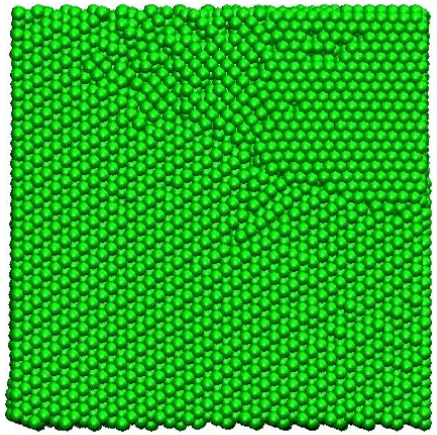

HMC Δt=8 fs N_{MD}=8

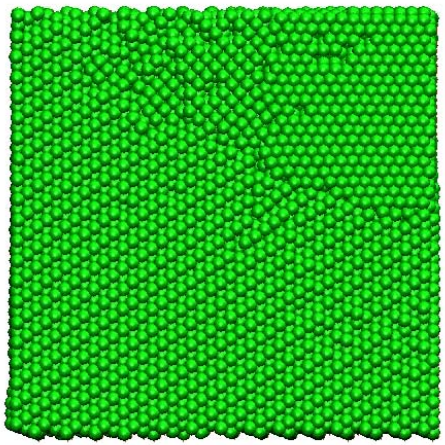

Time of Simulations for 9% Strain: Nanocrystalline Ni

CPU Time: Nanowire 15% Strain

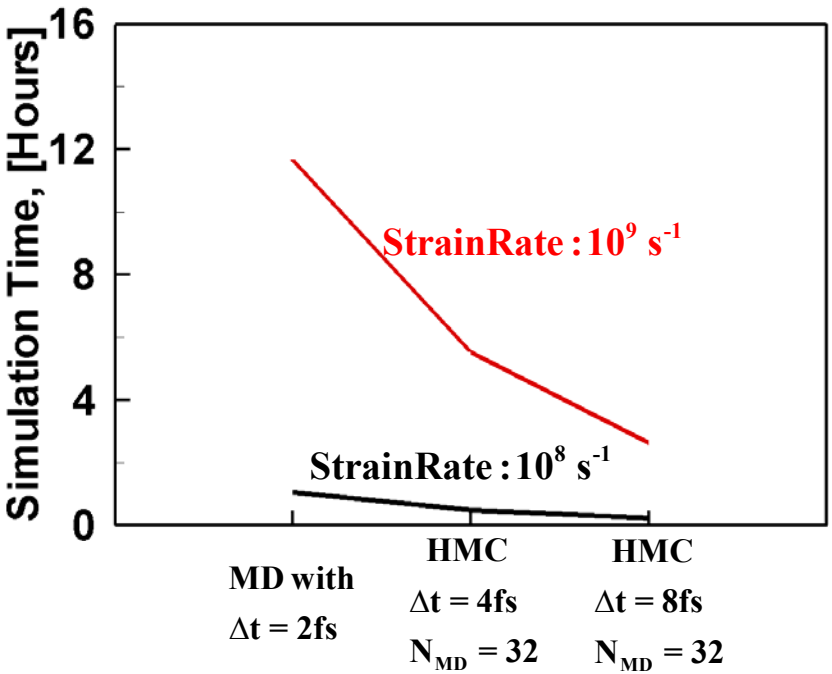

CPU Time: Nanocrystal 9% Strain

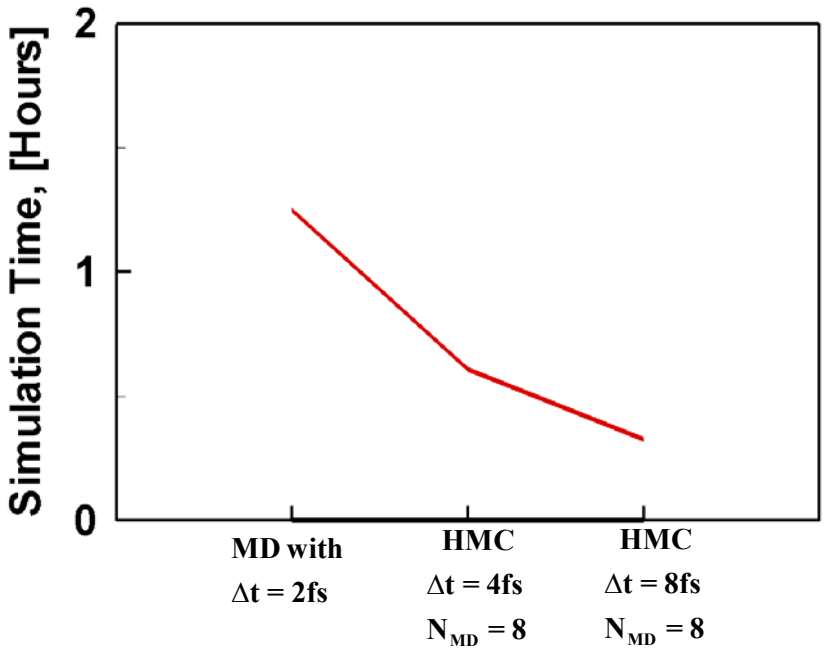

Summary

- Velocity profile different and therefore exact reproduction of defects as in MD impossible. However mechanistically the deformation maps agree with each other between MD and HMC
- Yield strain differ by about 0.1 fraction between MD and the most successful HMC case. This difference can be attributed to differences in the transition state events that trigger the propagation of defects in MD as well as in HMC. HMC events however have more statistical bias.
- Young's moduli, defect formation mechanisms, and yield strength always agree with each other very closely which are usually the main criterion for successful MD simulations
- Time gain is almost 4-32 times!
- Considering that MD nanostructural deformation have been used for deformation mechanism maps and mechanistic understanding, a huge and significant savings in times can be achieved by using HMC..

Outline

- Experiments and modeling of nanothermal behavior of SiC-Si_3N_4 nanocomposites with an account of hierarchy
  - The cohesive finite element method with focus on room temperature strength
  - Analyses of the effect of second phase particles and grain boundaries
- Analyzing superlattice interfaces for optimal thermal conduction problem in thermoelectricity
  - Molecular dynamic simulations to compute thermal diffusivity
  - Analyses of the effects of heat flow direction and grain size
- Achieving time-scaling by combining Molecular Dynamics and Monte Carlo in Hybrid Monte Carlo Method
- **Designing materials in an optimization framework**
  - **A variable fidelity model management framework**

Computer-aided design to investigate materials for use in future high temperature power plant applications

Design Targets

Fracture and creep resistance at about 1200 K

$SiC-Si_3N_4$

Design Variables

- Phase size
- Phase Volume Fraction

Variable Fidelity Optimization

Multiscale Material Simulation

Optimal Morphologies

$SiC-Si_3N_4$ nanocomposite with desired properties

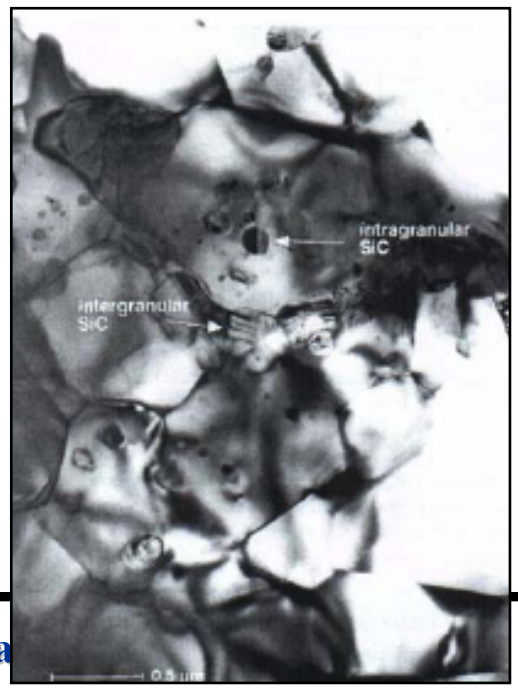

Want: Accuracy of quantum mechanics (QM) in 10^{23} atom systems…

This is impossible (today and in the foreseeable future)

Possible solution:
Multi-scale modeling techniques based on hierarchies of overlapping scales

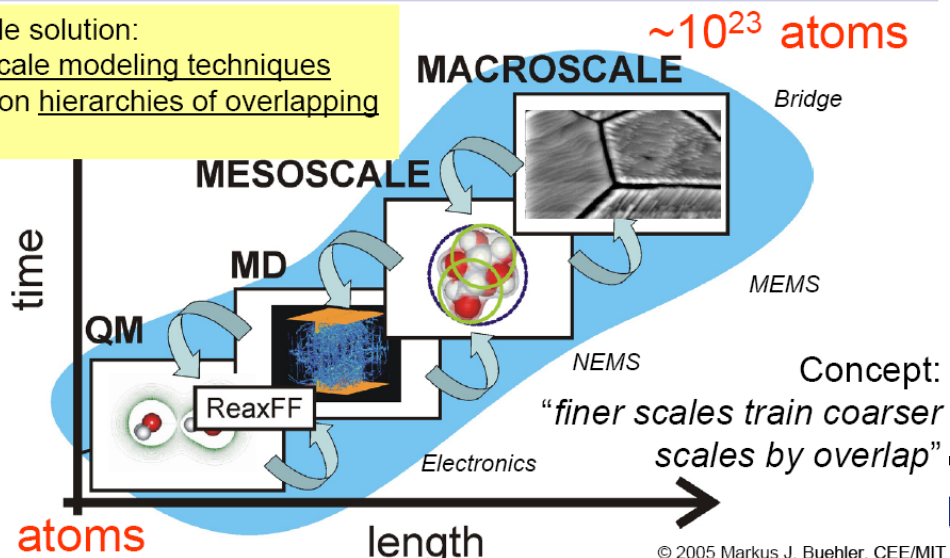

Concept:
"finer scales train coarser scales by overlap"

© 2005 Markus J. Buehler, CEE/MIT

Methodology for Materials Design

- **In systems design environments, various levels of model fidelity are developed**
  - **Low fidelity models**.
    - Drive the preliminary design process as surrogates of expensive high fidelity models.
    - Cheaper to evaluate.
  - **High fidelity models**
    - Used in the final design stages to refine the design.
    - At this stage may still require enormous computational resources.
- **Variable fidelity schemes incorporate both models into one optimization framework.**

Methodology for Materials Design

- **Low fidelity models are scaled to approximate the simulations results based on high fidelity models.**

- **Optimization can be performed by using mainly the low fidelity function calls, reducing the overall computational cost.**

- **Require only a few high fidelity evaluations to update a scaling function that drives the low fidelity function calls towards optimal design.**

Computer-aided design tool to improve $SiC\text{-}Si_3N_4$ composite fracture toughness and investigate materials performance

Construct scaling model

$$\beta(x) = \frac{f_{high}(x)}{f_{low}(x)} \rightarrow f_{high}(x) \approx \beta(x) f_{low}(x)$$

Optimize scaling model

maximize $\beta_n^1 K_{IC_{LOW}}(V_f, \theta)$,

subject to: $\beta_n^2 K_{I_{LOW}} \le \beta_n^1 K_{IC_{LOW}}(V_f, \theta)$,

$0 \le V_f \le 0.2$,

$0° \le \theta \le 90°$,

$-0.05 \le \Delta V_f \le 0.05$, and

$-4° \le \Delta\theta \le 4°$

Design Targets

Fracture resistance

Design Variables

- Second Phase orientation angle θ
- Second Phase Volume Fraction

Variable Fidelity Optimization

Simulation

Optimal Morphology

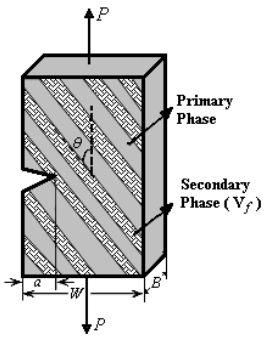

High fidelity model

CFCC setup modeled using COMSOL (FEM)

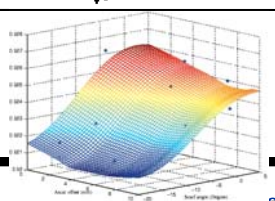

Low fidelity model

Response surface

Trust Region Variable Fidelity Optimization Framework

$$\beta(x) = \frac{f_{high}(x)}{f_{low}(x)} \Rightarrow f_{high}(x) \approx \beta(x) f_{low}(x)$$

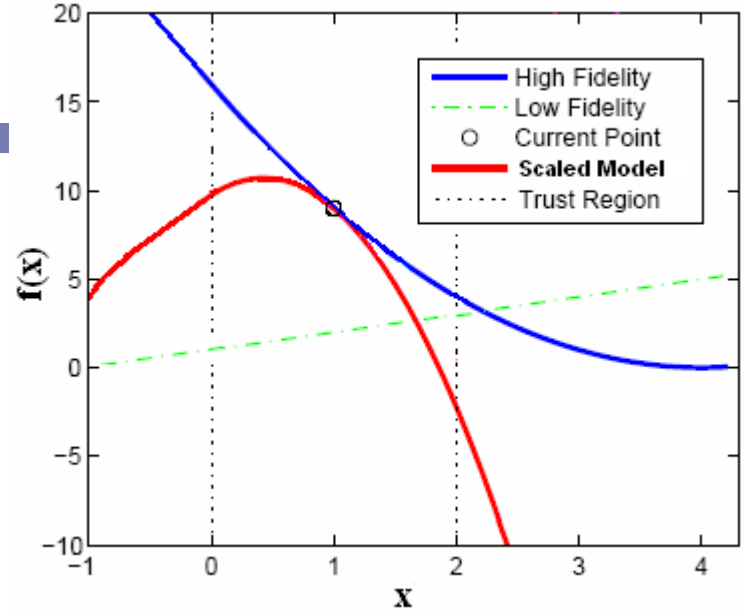

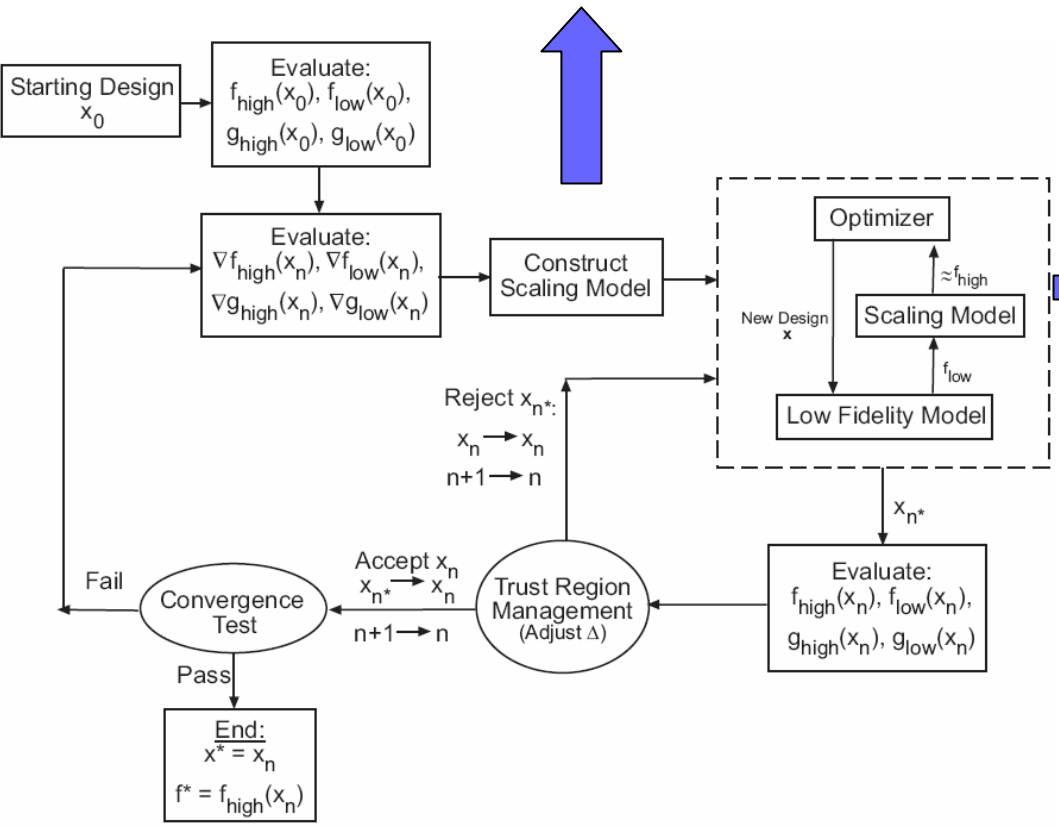

maximize $\beta_n^1 K_{IC_{LOW}}(V_f, \theta)$,

subject to: $\beta_n^2 K_{I_{LOW}} \le \beta_n^1 K_{IC_{LOW}}(V_f, \theta)$,

$0 \le V_f \le 0.2$,

$0° \le \theta \le 90°$,

$-0.05 \le \Delta V_f \le 0.05$, and

$-4° \le \Delta\theta \le 4°$

Find optimal CFCC configuration for improving K_{IC}

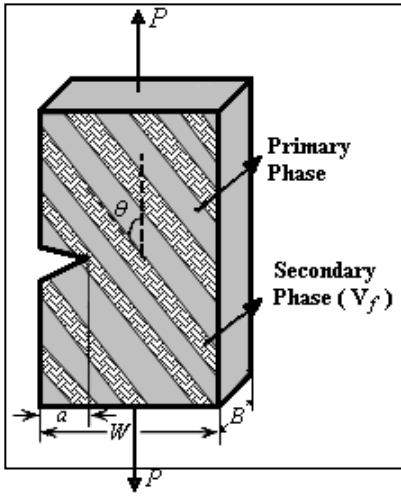

High fidelity model

CFCC setup modeled using COMSOL (FEM)

maximize Mode-I fracture toughness $K_{IC}\left(V_f,\theta\right)$

subject to:

$$K_I \le K_{IC}\left(V_f,\theta\right),$$

$$0 \le V_f \le 0.2, \text{ and}$$

$$0^\circ \le \theta \le 90^\circ.$$

The investigation was divided in the following three components:

- **Stress intensity factor calculation in the CFCC using the analytical fracture mechanics procedures (low fidelity) as well as by using finite element method (FEM) based analyses (high fidelity), to be used to satisfy the constraint in the optimization problem; and**
- **Fracture toughness calculation of the CFCC using finite element method (FEM) based analyses (high fidelity), as well as by using surrogate models (low fidelity) created from the high fidelity model; and**
- **Integration of the stress intensity factor and fracture toughness calculations at low and high fidelities into the trust region variable fidelity model management optimization framework.**

$$\Delta K_{IC} = \nabla K_{IC_1}\Delta(V_f) + \nabla K_{IC_2}\Delta(\theta) + \frac{1}{2}\left(H_{11}\Delta(V_f)^2 + H_{22}\Delta(\theta)^2\right) + H_{12}\Delta(V_f)\Delta(\theta)$$

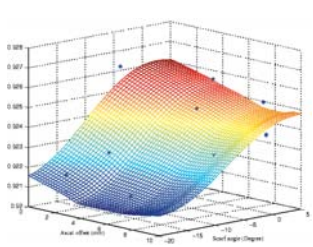

Low fidelity model

Response surface approximation

Optimization Method	Low Fidelity Simulations	High Fidelity Simulations	Iteration	θ^*(rad.)	V^*_f	$K_{IC}{}^*$(MPa·m$^{1/2}$)
Conventional	0	109	10	0.08528	0.2	7239246.361
Variable Fidelity	187	24	4	0.08531	0.2	7239245.175

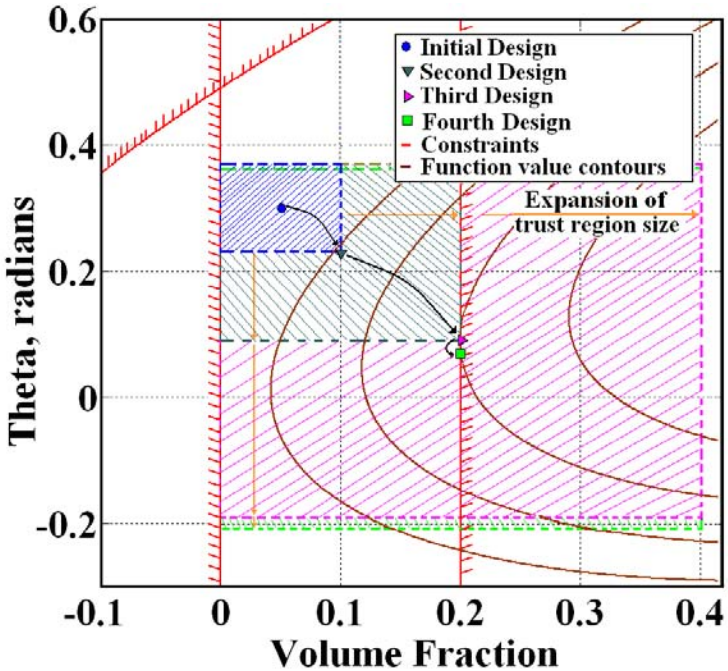

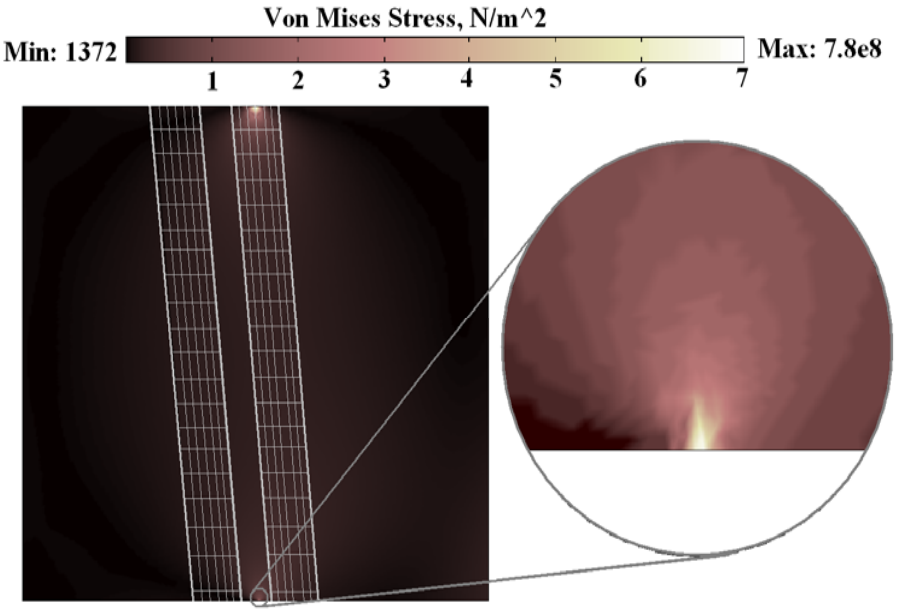

Initial design V_f^0 = 0.05 and θ^0 = 0.3 rad., and initial function value $K_{IC}{}^0$ = 7013519.592 MPa·m$^{1/2}$.

Iteration	Trust Region Adjustments	Trust Region Size		Convergence		Design Varibles and Obj. Function		
		$\Delta\theta$	ΔV_f	Δ_x	Δ_f	θ(rad.)	V_f	K_{IC} (MPa·m$^{1/2}$)
1	1	0.07	0.05	0.2828	0.0111	0.23	0.1	7091470.873
2	1	0.14	0.10	0.6859	0.0208	0.09	0.2	7239211.263
3	1	0.28	0.20	0.0214	4E-06	0.08530	0.2	7239241.029
4	10	2.1E-10	0.0000012	0.00002	6E-07	0.08531	0.2	7239245.175

Analysis of the effects of reinforcement size and volume fraction on the properties of these composites microstructure using CFEM (ABAQUS).

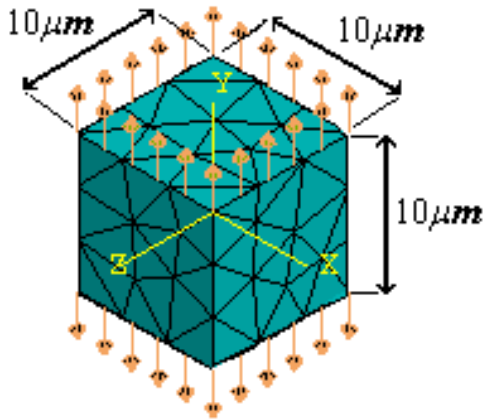

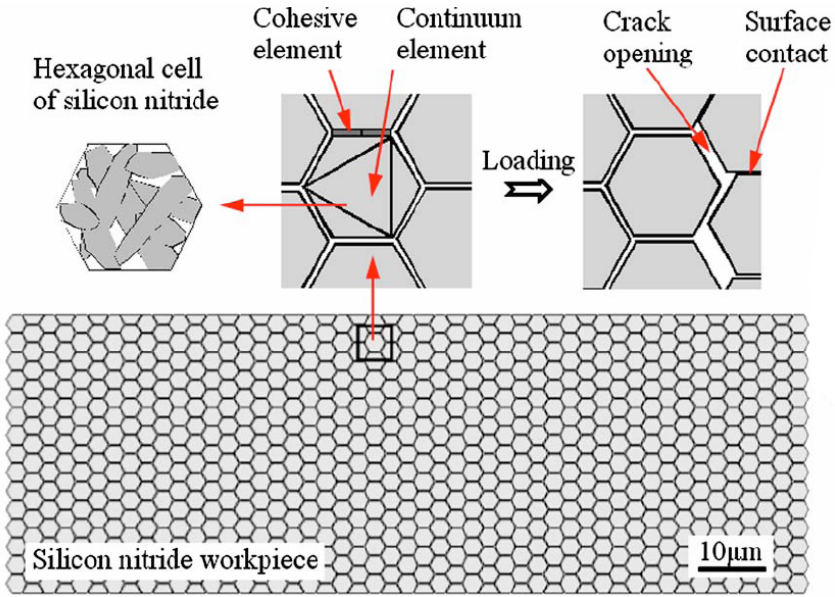

Illustration of the multiscale finite element modeling of silicon nitride. [Yinggang and Yung, 07]

$$\sigma = \sigma_0 \left[1 + \left(\frac{\varepsilon}{\varepsilon_0} \right)^n \right] \left[\frac{\dot{\varepsilon}}{\dot{\varepsilon}_0} \cdot \exp\left(\frac{Q}{RT} \right) \right]^m$$

σ_0 = reference flow stress, MPa
$\dot{\varepsilon}$ = strain rate, s^{-1}
$\dot{\varepsilon}_0$ = reference strain rate, s^{-1}
ε_0 = reference strain

Q = activation energy, kJ
R = universal gas constant, J/(mol K)
T = temperature, K
m = exponential coefficient of strain rate

Connect multiphysics models with variable input variables and fidelities

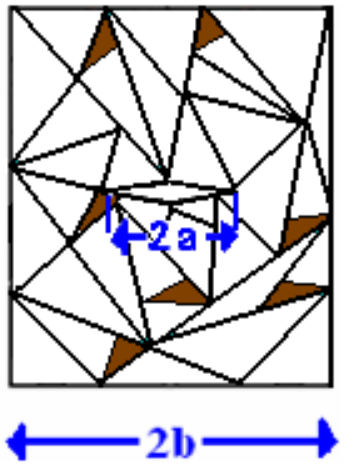

2D Low fidelity model

Design Variables

d- average grain size

T- temperature

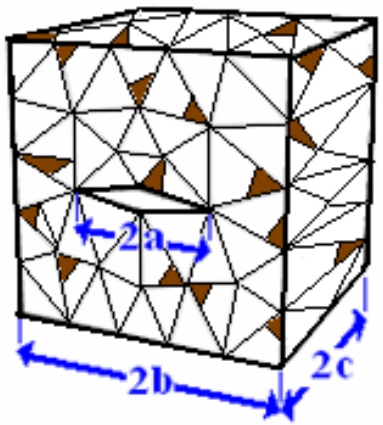

3D High fidelity model

Design Variables

d- average grain size

T- temperature

2c- thickness

Cohesive Model for Intergranular Glass Phase

- Temperature Dependant

$$F(\lambda) = \frac{27}{4} t_{n0}(T)(1-\lambda)^2$$

$$\lambda = \left[\left(\frac{\delta_n}{\delta_{n\,\max}} \right)^2 + \left(\frac{\delta_t}{\delta_{t\,\max}} \right)^2 \right]^{1/2}$$

$$t_{n0}(T) = t_0 \left[\frac{Q}{RT} - \ln(k_t \cdot t_F) \right]$$

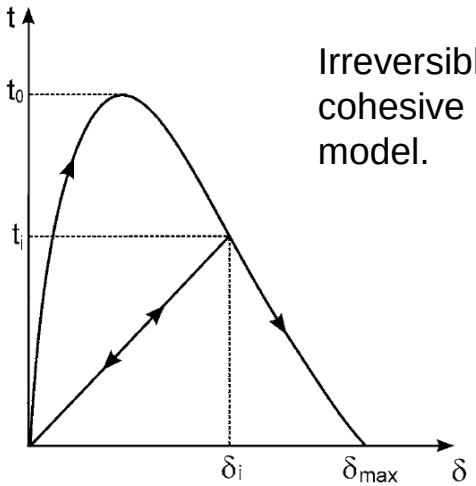

Irreversible cohesive model.

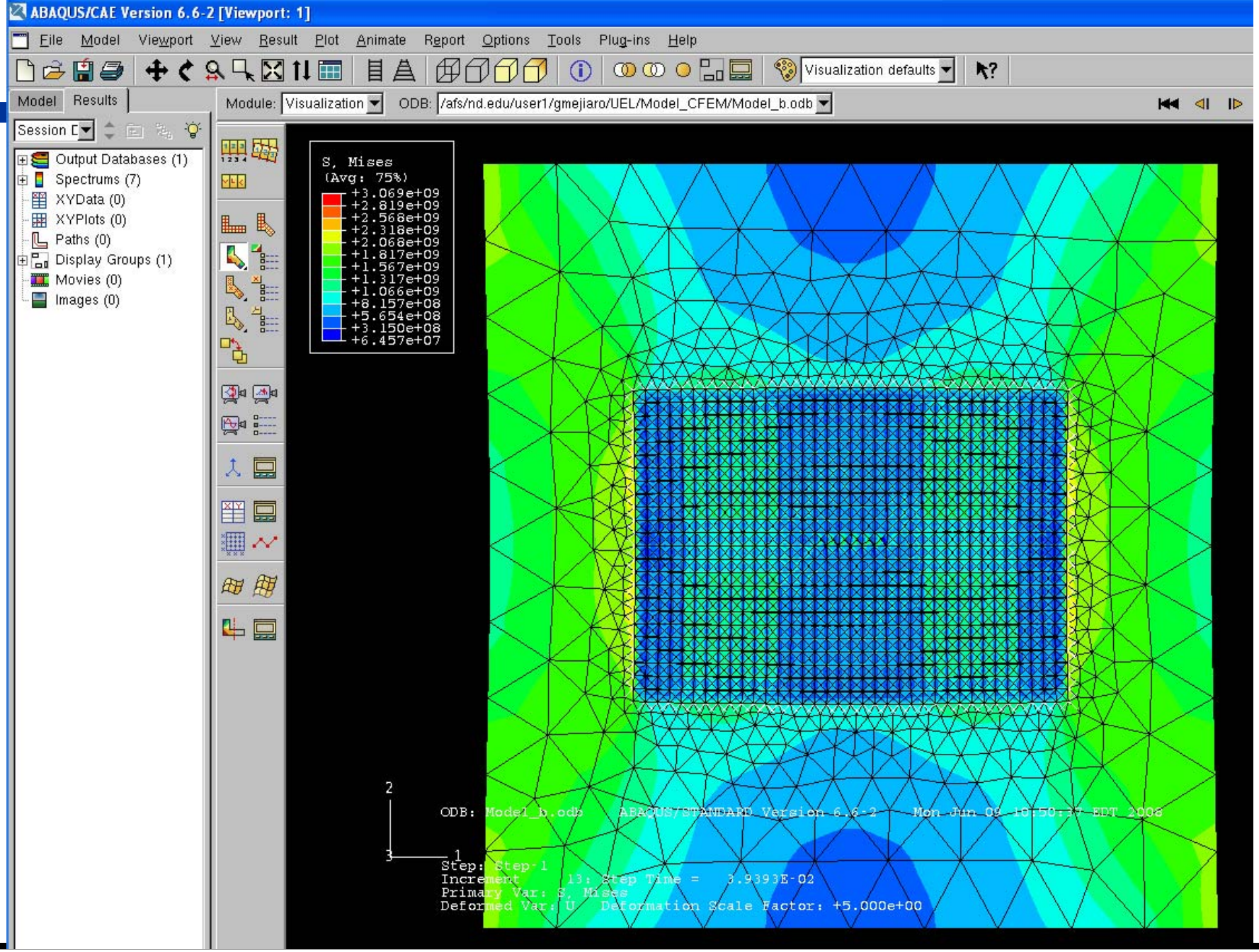
ABAQUS/CAE Version 6.6-2 [Viewport: 1]
File Model Viewport View Result Plot Animate Report Options Tools Plug-ins Help
Visualization defaults
Model Results
Module: Visualization
ODB: /afs/nd.edu/user1/gmejiaro/UEL/Model_CFEM/Model_b.odb
Output Databases (1)
Spectrums (7)
XYData (0)
XYPlots (0)
Paths (0)
Display Groups (1)
Movies (0)
Images (0)
S, Mises
(Avg: 75%)
+3.069e+09
+2.819e+09
+2.568e+09
+2.318e+09
+2.068e+09
+1.817e+09
+1.567e+09
+1.317e+09
+1.066e+09
+8.157e+08
+5.654e+08
+3.150e+08
+6.457e+07
ODB: Model_b.odb ABAQUS/STANDARD Version 6.6-2 Mon Jun 09 10:50:17 EDT 2008
Step: Step-1
Increment 13: Step Time = 3.9393E-02
Primary Var: S, Mises
Deformed Var: U Deformation Scale Factor: +5.000e+00

Summary

- **Coal will become the energy and raw material resource of choice in the coming decades. The key is developing technologies for clean coal utilization.**

- **It is estimated that the use of bulk materials ($SiC-Si_3N_4$) with high temperature properties to operate at temperatures in excess of 1500 °C in power plants can result in enhancements in the power generation efficiency by 10% to 15%.**

- **The Computer Aided Multiscale Design tool is expected to work efficiently on obtaining the most suitable sets of morphologies (design variables) to obtain a designated target set of properties by integrating multiscale simulations of the $SiC-Si_3N_4$ nanocomposite in a trust region variable fidelity framework.**

- **Results will be useful for understanding the applicability of this important class of materials to future fossil energy conversion systems.** ***The demand for higher efficiency and reduced emissions in advanced fossil-fuel conversion systems will require materials with higher oxidation, corrosion, creep, and fracture resistance at high temperatures.***

- **We would like to once again thank DoE for the support.**
- **Journal Publications**

1. **Mejia-Rodriguez, G., Renaud, J.E., and Tomar V., 2008, A variable fidelity model management framework for designing multiphase materials, *to appear in the ASME Journal of Mechanical Design***

2 **Tomar, V., 2008, Analyses of the role of the second phase SiC particles in microstructure dependent fracture resistance variation of SiC-Si_3N_4 nanocomposites, *Modelling Simul. Mater. Sci. Eng. 16 (2008) 035001.***

3 **Tomar, V., 2007, Nanomechanical analyses of nanocrystalline Ni using accelerated molecular timesteps, Physica Status Solidi-a, vol. 204 (10), pp. 3340-3348.**

4 **Tomar, V., 2007, Accelerating the molecular timesteps for nanomechanical simulations: The hybrid Monte Carlo Method, Journal of Applied Physics, Vol. 101, pp 103512 (1-9)**